NICST Internal Memo

Date: February 25, 2011
From: Jeff McIntire
To: Bruce Guenther, Jim Butler, and Jack Xiong
Subject: Plateau and Electronics Side Comparison of Thermal Band Radiometric Calibration from VIIRS F1 RC-05 Testing

---

References:

[1] 'Sensor Performance Verification Plan,' PVP154640-101.
[2] 'Performance Specification Sensor Specification,' ps154640-101c.
[3] NICST_MEMO_11_001, 'Analysis of the Radiometric Calibration from VIIRS F1 RC-05 Part 1 Test (Nominal Plateau, Electronic Side B),' Jeff McIntire and Sanxiong Xiong, January 3, 2011.
[4] NICST_MEMO_11_002, 'Analysis of the Radiometric Calibration from VIIRS F1 RC-05 Part 2 Test (Nominal Plateau),' Jeff McIntire and Sanxiong Xiong, January 31, 2011.
[5] IT_OBCBB_EDU_Temp_081112, 'OBC Blackbody Temperature Calculation,' Courtney Ranshaw, November 11, 2008.

1. Introduction

During the thermal vacuum testing of VIIRS F1 sensor, RC-05 was performed under a variety of instrument conditions. RC-05 Parts 1 and 2 were conducted at three instrument temperature plateaus (Cold, Nominal, and Hot). In addition, RC-05 Part 1 was tested using both electronics sides A and B at each plateau. The purpose of this memo is to compare and trend the thermal band performance across different instrument conditions, including compliance with a number of specifications [1,2].

The methodology, processing, and results of RC-05 at Nominal plateau, electronic side B have been reported for both Parts 1 and 2 [3,4]. Tables 1 - 7 list the data used in this work. Tables 1 – 6 contain the data from RC-05 Part 1 (all plateaus and electronics sides) used in the high gain determination on the left and the low gain determination on the right. All UAIDs, collects, gain modes, and relevant source temperatures are listed. Table 7 lists the RC-05 Part 2 data for both warm up and cool down at all three instrument temperature plateaus. Note that Part 2 data taken at Cold plateau was on electronics side A and data taken at Nominal and Hot plateaus was on electronics side B. The results shown in this work are from HAM side A (HAM sides A and B yield similar results).

2. Analysis

2.1 RC-05 Part 1 High Gain (BCS source)

The radiometric coefficient a_0 for each high gain band is plotted in Figure 1 versus detector for all plateaus and electronics sides. In general, the a_0 coefficient is on the order of 10^{-2} or less and is roughly consistent over plateaus and electronic sides. M14 has the largest offset of around 0.01 – 0.02 for all detectors. The detector dependence is fairly stable versus instrument condition for the LWIR; some variation is observed in the MWIR. In addition, the detector 1 offset seems to be Out Of Family (OOF) in the LWIR. In Figure 2, the a_0 coefficients for the all detectors in each band are graphed versus T_{OMM} temperature (solid lines for electronics side A and dashed lines for electronics side B). There is a good deal of detector variation in the a_0 trends versus T_{OMM}. However, it should be noted that the variation of the offset with plateau is on the order of 10^{-2} or less. Figure 3 shows the same trend versus T_{OMM} for a middle detector (8 for M bands and 16 for I bands) along with 2 sigma error bars (NIST standard). Note that in general the error bars overlap for the different plateaus (electronics side dependent), and as a result, a_0 is consistent over instrument temperature conditions. For almost all bands and detectors, the error bars overlap across all instrument conditions.

Figure 4 contains the gains ($1/a_1$) for all high gain bands (all plateaus and electronics sides). The detector to detector patterns are very consistent from plateau to plateau and across electronics side. Also, note that strong odd – even detector dependence is observed in I5, M12, and M13 and that M12 detector 1 is consistently OOF. The gain trends versus T_{OMM} are shown in Figure 5. The gains trend fairly linearly over plateau. In addition, the gains tend to decrease with T_{OMM}, with the exception of M13, which registers a slight increase. In general, the LWIR bands decrease by about 2 % or less and the MWIR bands change by less than 1 % over the ~16 K T_{OMM} range. Figure 6 shows the gain trend for a middle detector versus T_{OMM} along with the 2 sigma error bars. Here the temperature variation is outside the error bars in most cases, particularly for the LWIR bands. There is some overlap between plateaus for a given electronics side for I4 and M13, but the electronics sides are not consistent.

The nonlinear term a_2 is plotted in Figure 7 for all high gain bands (across plateaus and electronics sides). For the LWIR bands, the detector pattern of the nonlinear term is roughly constant over plateau and electronics side; however, for the MWIR, the pattern is less well defined. In terms of magnitude, the nonlinear term is consistently below 10^{-8}. In Figure 8, the trending versus T_{OMM} for a_2 is shown (all detectors). For most bands and electronics sides, the nonlinear term exhibits a small, roughly linear increase with T_{OMM} (less well defined for the MWIR bands). There is some noticeable detector variation in the trending for the MWIR. The a_2 trend versus T_{OMM} is plotted in Figure 9 for a middle detector along with the 2 sigma error bars. For the majority of cases, the error bars overlap. The most glaring exceptions are in I4, M12, and M14.

The NEdT at T_{TYP} for high gain bands, plateaus, and electronics sides is shown in Figure 10. The NEdT at T_{TYP} is very consistent over the range of instrument conditions tested, both in terms of magnitude and detector dependence. Note that detectors 31 in I5, 1 in M12, and 8 in M16A are consistently OOF. Figure 11 shows the dependence on T_{OMM} for the NEdT at T_{TYP} (all detectors). The NEdT generally increases with T_{OMM} for all bands and both electronics sides (although there is a good deal of detector dependence). This is the result of the increasing dark noise in the detectors which occurs at higher instrument temperatures. The NEdT at T_{TYP} increases about 10 % over the T_{OMM} range of ~16 K (except for M12 which increases roughly 30 %). The NEdT as a function of BCS temperature is graphed in Figure 12 for all high gain bands and instrument conditions (median detector). Again, the NEdT is consistent across instrument conditions, excepting the slight increase with instrument temperature due to increasing dark noise. Note that only the data within the optimized dynamic range is plotted here [3] (the optimized M14 dynamic range begins at 210 K, which was only measured once).

The nonlinearity metric (RRNL) is graphed versus detector for all instrument conditions in Figure 13. The RRNL is generally consistent over instrument conditions. The exception is M14; the Nominal plateau, electronics side B set includes a larger set of BCS levels including 210 K (at all other instrument conditions, this data point is not measured). As a result, the fitting for M14 is more tightly constrained for Nominal plateau, electronics side B.

The ARD for all bands and instrument conditions is shown in Figure 14 (median detector). The ARD are roughly consistent over all plateaus and electronics sides for the optimized dynamic range. In the MWIR, there is a constant bias of about 0.3 % which results from the application of the scan by scan OBC correction to the retrieved radiance (see [3]). In addition, the shape that is present in the MWIR is largely the result of the radiometric fitting.

The potential for detector to detector striping was measured by the RRU, graphed for all bands, plateaus, and electronics sides in Figure 15 (worst case detector). A RRU greater then one indicates the potential for striping (dashed red line in the plots). The RRU generally increases with increasing scene temperature. For bands I4, M12, M13, M14, and M15, some striping is possible at the highest scene temperatures. Note that the specification is only valid between the specified L_{MIN} and $0.9L_{MAX}$. Most of the evidence for striping occurs above that range. At higher temperatures, the deviation of the retrieved radiance from the band average increases, but the measured NEdL levels off; the result is a steadily increasing RRU.

2.2 RC-05 Part 1 Low Gain (TMC source)

The M13 low gain coefficients for all bands, plateaus, and electronics sides are shown in Figure 16. The detector patterns are consistent over instrument conditions for both a_1 and a_2; in contrast, no discernable pattern exists for a_0, which is generally consistent with zero. The temperature trends for each coefficient (all detectors) are graphed in Figure 17. For electronics side B, $1/a_1$ tends to decrease linearly with T_{OMM} and a_2 tends to increase with T_{OMM}. However, no such dependence is evident for electronics side A. The gain varies by up to 5 % over instrument conditions while a_2 is on the 10^{-7} level. The coefficient trends versus T_{OMM} with 2 sigma error bars (middle detector) are shown in Figure 18. In general, the error bars overlap for a_0, but not for a_1 or a_2. Note that this uncertainty is in part due to the difficulty in cross calibrating the TMC to the BCS and to the fact that only five scene temperatures were measured for the low gain dynamic range (optimized).

The NEdT is plotted in Figure 19 for M13 low gain. In the left hand plot, the NEdT at T_{TYP} is shown versus detector for all instrument conditions. The NEdT at T_{TYP} is not very consistent from detector to detector or from instrument condition to instrument condition. This results from the fact that T_{TYP} is 380 K for M13 low gain, and that this is a portion of the dynamic range that was under-sampled during testing. In consequence, the NEdT at T_{TYP} is difficult to constrain. Nonetheless, all detectors meet the requirement (red dashed line) for all instrument conditions. The right hand plot in Figure 19 shows the NEdT as a function of effective TMC temperature (the blackbody temperature associated with the retrieved TMC radiance). The NEdT is between 0.1 and 0.2 K above about 450 K; below this the NEdT increases to as much as 0.5 K near 350 K.

Figure 20 shows some of the performance metrics associated with M13 low gain. In the left hand plot, the nonlinearity metric is graphed versus detector for all instrument conditions. The nonlinearity is consistent over all plateaus and electronics sides, and is well within the specified limit (dashed red line). The middle graph contains the M13 low gain ARD versus effective TMC temperature (worst case detector). The ARD is consistent over instrument conditions above about 450 K; below this there is some discrepancy between the data collections. In the rightmost plot, the RRU is graphed versus effective TMC temperature (worst case detector). Some potential striping is evident at lower instrument temperatures in the region around 500 K, but is not observed at higher instrument temperatures.

2.3 RC-05 Part 2 High Gain (OBC source)

The OBC warm up and cool down cycle was performed at all three instrument temperature plateaus. However, it was only measured on one electronics side per plateau: A side for Cold plateau and B side for Nominal and Hot plateaus. It should be noted that the number of OBC levels is not the same for warm up and cool down (cool down has three less levels at lower temperature than warm up for the same plateau). In addition, the number of levels changes from plateau to plateau: warm up at Cold plateau has one more level then warm up at Nominal plateau and two more levels than warm up at Hot plateau, all at lower temperatures (similarly for cool down). As a result, any plateau comparison must take into account the fact that the temperature range used in the fitting was not consistent across RC-05 Part 2 measurements.

The coefficient a_0 derived from the OBC warm up is plotted versus detector for all high gain bands and plateaus in Figure 21. The pattern over detectors is not consistent from plateau to plateau. The additional levels at colder instrument temperatures are a large constraint on the fitting, especially the offset term. Figure 22 shows the trend versus

T_{OMM} for all bands (median detector). In most cases the relationship is nonlinear, but is within the expanded (2 sigma) error bars.

The OBC warm up gain is graphed versus detector for all high gain bands and plateaus in Figure 23. The detector pattern is consistent over the three plateaus. The median detector gain trend versus T_{OMM} is shown in Figure 24. In general, the gains have a roughly linear relationship with T_{OMM}; one exception is M12, which appears to have a more nonlinear trend. The gain variation with T_{OMM} is roughly less than 1 % (MWIR) or 2 % (LWIR) over about 16 K. In general, the gains are not consistent over instrument conditions (excepting I4, I5, and M15).

Figure 25 shows the detector variation in the coefficient a_2 for all high gain bands and plateaus. As with a_0, the detector to detector variation in a_2 is generally not consistent from plateau to plateau. As noted before, the additional low temperature levels are a large constraint on the fitting, especially affecting both the offset and nonlinear terms (particularly in the MWIR). The median detector a_2 trend versus T_{OMM} is plotted in Figure 26 and shows a nonlinear relationship for all bands. However, the trend is within the 2 sigma expanded uncertainties for all bands.

In contrast to the OBC warm up gains, Figure 27 graphs the OBC cool down gains versus detector for all plateaus. The detector patterns are less well defined compared the warm up gains (see Figure 23). The number of levels available in the cool down portion of the cycle is three less than the warm up at any given plateau. In addition, the extra levels that are available in warm up are at lower temperatures. Thus, the ability to constrain the fitting in the cool down cycle is significantly reduced.

The NEdT at T_{TYP} derived from both OBC warm up and cool down is shown for all bands versus detector in Figure 28. The NEdT at T_{TYP} is generally consistent over plateau and electronics side. In the case of I5, Hot plateau warm up shows some deviation from the other data collections; for I5, T_{TYP} is 210 K (well below the measured range) and the extrapolation may not be well constrained. In addition, a slight increase in NEdT over instrument temperature is observed (consistent with increasing dark noise).

Figure 29 plots the BCS ARD for both warm up and cool down for all three plateaus versus T_{OBC}. In general, the warm up and cool down ARD tend to decrease with increasing T_{OBC}. In addition, the warm up ARD trend slightly higher with instrument temperature. The cool down ARD are offset from the warm up ARD by about 0.1 % in the MWIR and 0.05 % in the LWIR.

The deviation from the specified OBC temperature setpoint is shown in Figure 30 as a function of T_{OBC}. The dashed red lines indicate the allowed tolerance of ±0.2 K (SRV0654). The deviation exceeds the tolerance as T_{OBC} decreases below 292 K for all plateaus. This is in part due to the updated OBC temperature calculation [5], which was not used to set the OBC temperature during testing. This correction increases as T_{OBC} decreases. In Figure 31, the standard deviation of the temperatures extracted from the six thermistors imbedded in the OBC is plotted versus T_{OBC}. The specification requires this standard deviation to be below 0.03 K (SRV0095) for temperature controlled conditions (warm-up). The standard deviation meets this requirement for all scene temperatures and plateaus.

3. Summary

- External source (BCS) – high gain
    - The a_0 coefficients are on the order of 10^{-2} or less and are consistent over both electronics side and instrument temperature plateau (within 2 sigma).
    - The a_2 coefficients are consistently below 10^{-8} and are largely within the 2 sigma errors.
    - In general, the gains trend lower with increased instrument temperature (about 2 % or less). The exception is M13, which exhibits a slight increase. The trends are largely outside the 2 sigma errors.
    - Detector to detector differences in the gain are consistent over all instrument conditions. Odd – even dependence is observed in I5, M12, and M13.
    - The NEdT at T_{TYP} is consistent across instrument conditions, excepting the slight increase with instrument temperature due to increasing dark noise (roughly a 10 % increase over the measured range).
    - The nonlinearity metric is consistent over all instrument conditions.
    - The ARD is consistent over all instrument conditions within the dynamic range. There is a small bias in the MWIR bands due to the scan by scan OBC correction.
    - The potential for detector to detector striping increases with scene temperature consistently over instrument conditions, with striping resolved from the noise observed at the highest measured scene temperatures for bands I4, M12, M13, M14, and M15.
- External source (TMC) – low gain
    - The coefficient a_0 is consistent with zero for all measurements. The gain varies by up to 5 % (which is outside the 2 sigma uncertainty). The a2 coefficient increases with instrument temperature and is generally inconsistent over instrument conditions.
    - The NEdT at T_{TYP} is not very consistent across instrument conditions, but is nonetheless below the specified limit.
- Internal source (OBC) – high gain
    - The warm-up a_0 and a_2 coefficients are consistent over plateaus within the expanded uncertainty.
    - The warm-up gains are also consistent over instrument conditions within the 2 sigma uncertainty (except for bands M12 and M13). The gains trend lower by about 2 % (except for bands M12 and M13, which trend higher by about 1 %). Cool-down gains are less well defined.
    - The NEdT at T_{TYP} is consistent over instrument plateaus (excepting a slight increase due to increasing dark noise) and well within the specification.

- The BCS ARD tends to decrease slightly with increasing T_{OBC}. In addition, the cool-down ARD is slightly higher than the warm-up.
- The standard deviation of the six OBC thermistors is below 0.03 K for all instrument conditions.

Acknowledgement

The sensor test data used in this document was provided by the Raytheon El Segundo testing team. Approaches for data acquisition and data reductions, as well as data extraction tools were also provided by the Raytheon El Segundo team. We would like to thank the Raytheon El Segundo team for their support. The data analysis tools were developed by the NICST team.

Table 1: F1 RC-05 Part 1 data (Cold plateau, electronics side A)

High gain					Low gain				
UAID	Collect	Gain Mode	T_OBC (K)	T_BCS (K)	UAID	Collect	Gain Mode	T_TMC (K)	T_BCS (K)
U3103363	2	high	292.6	189.7	U3103363	1	high	293.3	189.6
U3103363	4	high	292.6	230.1	U3103363	3	high	296.0	230.1
U3103363	6	high	292.6	247.1	U3103363	5	high	293.1	247.1
U3103363	8	high	292.6	262.1	U3103363	7	high	293.1	262.1
U3103363	10	high	292.6	278.2	U3103363	9	high	293.1	278.2
U3103363	13	high	292.6	292.1	U3103363	14	high	293.3	292.1
U3103363	16	high	292.6	306.8	U3103363	15	high	315.1	306.8
U3103363	18	high	292.6	321.0	U3103363	17	high	334.1	321.0
U3103363	20	high	292.6	332.0	U3103363	19	high	348.1	332.0
U3103363	22	high	292.6	340.1	U3103363	21	high	358.1	340.1
U3103363	24	high	292.6	345.1	U3103363	23	high	364.1	345.0
					U3103364	1	low	378.1	345.1
					U3103364	4	low	563.2	345.1
					U3103364	7	low	638.2	345.1
					U3103364	13	low	688.1	345.1
					U3103364	16	low	718.1	345.1

Table 2: F1 RC-05 Part 1 data (Nominal plateau, electronics side A)

High gain					Low gain				
UAID	Collect	Gain Mode	T_OBC (K)	T_BCS (K)	UAID	Collect	Gain Mode	T_TMC (K)	T_BCS (K)
U3103556	2	high	292.6	190.0	U3103556	1	high	815.2	190.0
U3103556	4	high	292.6	230.0	U3103556	3	high	325.9	230.0
U3103556	7	high	292.6	247.3	U3103556	5	high	306.7	247.3
U3103556	9	high	292.6	262.3	U3103556	8	high	297.6	262.2
U3103558	2	high	292.6	278.2	U3103558	1	high	293.2	278.2
U3103558	4	high	292.6	292.4	U3103558	3	high	305.1	292.4
U3103558	6	high	292.6	307.2	U3103558	5	high	325.1	307.2
U3103558	8	high	292.6	321.3	U3103558	7	high	344.1	321.3
U3103558	10	high	292.6	332.4	U3103558	9	high	358.1	332.3
U3103558	12	high	292.6	340.4	U3103558	11	high	369.1	340.4
U3103558	15	high	292.6	345.2	U3103558	14	high	375.1	345.2
					U3103560	1	low	388.1	345.2
					U3103560	5	low	599.2	345.2
					U3103560	8	low	677.2	345.2
					U3103560	11	low	730.2	345.2
					U3103560	14	low	763.2	345.2

Table 3: F1 RC-05 Part 1 data (Hot plateau, electronics side A)

High gain					Low gain				
UAID	Collect	Gain Mode	T_OBC (K)	T_BCS (K)	UAID	Collect	Gain Mode	T_TMC (K)	T_BCS (K)
U3104466	2	high	292.6	190.0	U3104466	1	high	292.7	190.0
U3104466	4	high	292.6	230.1	U3104466	3	high	293.1	230.1
U3104466	6	high	292.6	247.2	U3104466	5	high	293.1	247.2
U3104466	8	high	292.6	262.2	U3104466	7	high	293.1	262.2
U3104466	10	high	292.6	278.2	U3104466	9	high	293.1	278.2
U3104466	13	high	292.6	292.3	U3104466	11	high	305.2	292.3
U3104466	15	high	292.6	307.1	U3104466	14	high	325.1	307.1
U3104466	17	high	292.6	321.3	U3104466	16	high	344.1	321.3
U3104466	19	high	292.6	332.2	U3104466	18	high	358.1	332.2
U3104466	21	high	292.6	340.2	U3104466	20	high	369.1	340.2
U3104466	24	high	292.6	345.4	U3104466	22	high	375.2	345.4
					U3104467	1	low	388.2	345.3
					U3104467	6	low	599.2	345.3
					U3104467	10	low	677.2	345.3
					U3104467	13	low	730.2	345.2
					U3104467	16	low	763.1	345.2

Table 4: F1 RC-05 Part 1 data (Cold plateau, electronics side B)

High gain					Low gain				
UAID	Collect	Gain Mode	T_OBC (K)	T_BCS (K)	UAID	Collect	Gain Mode	T_TMC (K)	T_BCS (K)
U3103519	2	high	292.7	190.0	U3103519	1	high	394.7	190.0
U3103519	4	high	292.7	230.1	U3103519	3	high	293.6	230.1
U3103520	2	high	292.7	247.1	U3103520	5	high	293.3	247.1
U3103520	4	high	292.7	262.3	U3103520	7	high	293.0	262.3
U3103520	6	high	292.7	278.1	U3103520	9	high	293.1	278.1
U3103520	9	high	292.7	292.2	U3103520	11	high	293.1	292.2
U3103520	11	high	292.7	306.9	U3103520	14	high	315.1	306.9
U3103520	13	high	292.7	321.2	U3103520	16	high	334.1	321.2
U3103520	15	high	292.7	332.2	U3103520	18	high	348.2	332.2
U3103520	17	high	292.7	340.2	U3103520	20	high	358.1	340.2
U3103520	19	high	292.7	345.0	U3103520	22	high	364.1	345.0
					U3103522	1	low	378.1	345.0
					U3103522	6	low	563.2	345.0
					U3103522	10	low	638.1	345.1
					U3103522	13	low	688.1	345.1
					U3103522	16	low	718.1	345.1

Table 5: F1 RC-05 Part 1 data (Nominal plateau, electronics side B)

High gain					Low gain				
UAID	Collect	Gain Mode	T_OBC (K)	T_BCS (K)	UAID	Collect	Gain Mode	T_TMC (K)	T_BCS (K)
U3103773	2	high	292.6	190.0	U3103773	1	high	292.4	190.0
U3103773	4	high	292.7	210.3	U3103773	3	high	293.1	210.3
U3103773	6	high	292.7	230.3	U3103773	5	high	293.1	230.3
U3103773	8	high	292.7	240.2	U3103773	7	high	293.1	240.2
U3103773	10	high	292.7	247.1	U3103773	9	high	293.1	247.1
U3103773	12	high	292.7	255.4	U3103773	11	high	293.1	255.4
U3103773	14	high	292.7	261.8	U3103773	13	high	293.1	261.8
U3103773	16	high	292.7	269.9	U3103773	15	high	293.1	269.9
U3103773	18	high	292.7	278.2	U3103773	17	high	293.1	278.2
U3103773	21	high	292.7	285.3	U3103773	19	high	293.1	285.3
U3103773	23	high	292.7	292.2	U3103773	22	high	305.1	292.2
U3103773	25	high	292.7	300.2	U3103773	24	high	316.1	300.2
U3103773	27	high	292.7	307.2	U3103773	26	high	325.1	307.2
U3103773	29	high	292.7	315.3	U3103773	28	high	336.1	315.3
U3103773	31	high	292.7	321.3	U3103773	30	high	344.1	321.3
U3103773	33	high	292.7	327.3	U3103773	32	high	351.1	327.3
U3103773	35	high	292.7	332.3	U3103773	34	high	358.1	332.3
U3103773	37	high	292.7	336.3	U3103773	36	high	363.1	336.3
U3103773	39	high	292.7	340.4	U3103773	38	high	369.1	340.4
U3103773	41	high	292.7	345.3	U3103773	40	high	375.1	345.3
					U3103775	1	low	388.2	345.2
					U3103775	5	low	539.2	345.2
					U3103775	8	low	599.2	345.2
					U3103775	11	low	645.2	345.2
					U3103775	14	low	677.2	345.2
					U3103775	17	low	704.1	345.2
					U3103775	20	low	730.2	345.2
					U3103775	23	low	763.2	345.2

Table 6: F1 RC-05 Part 1 data (Hot plateau, electronics side B)

High gain					Low gain				
UAID	Collect	Gain Mode	T_OBC (K)	T_BCS (K)	UAID	Collect	Gain Mode	T_TMC (K)	T_BCS (K)
U3104327	2	high	292.7	190.1	U3104327	1	high	293.3	190.1
U3104327	4	high	292.7	230.3	U3104327	3	high	292.9	230.3
U3104327	6	high	292.7	247.2	U3104327	5	high	293.1	247.2
U3104327	8	high	292.7	261.9	U3104327	7	high	293.1	261.9
U3104327	10	high	292.7	278.2	U3104327	9	high	293.1	278.2
U3104327	12	high	292.7	292.3	U3104327	11	high	305.2	292.3
U3104327	14	high	292.7	307.1	U3104327	13	high	325.1	307.1
U3104327	17	high	292.7	321.3	U3104327	15	high	344.1	321.3
U3104327	19	high	292.7	332.4	U3104327	18	high	358.2	332.4
U3104327	22	high	292.7	340.4	U3104327	20	high	369.2	340.4
U3104327	24	high	292.7	345.3	U3104327	23	high	375.1	345.3
					U3104328	1	low	388.2	345.2
					U3104328	5	low	599.2	345.2
					U3104328	8	low	677.2	345.2
					U3104328	14	low	730.1	345.2
					U3104328	20	low	763.2	345.2

Table 7: F1 RC-05 Part 2 data

Cold Plateau				Nominal Plateau				Hot Plateau			
UAID	Collect	T_OBC (K)	T_BCS (K)	UAID	Collect	T_OBC (K)	T_BCS (K)	UAID	Collect	T_OBC (K)	T_BCS (K)
U3103451	1	260.8	300.2								
U3103451	2	273.0	300.2	U3103908	1	273.0	300.1				
U3103451	3	282.9	300.2	U3103908	2	282.9	300.1	U3104416	1	282.9	300.3
U3103451	4	292.7	300.2	U3103908	3	292.8	300.1	U3104416	2	292.7	300.3
U3103451	5	297.6	300.2	U3103908	4	297.7	300.1	U3104416	3	297.7	300.3
U3103451	6	302.5	300.2	U3103908	5	302.6	300.1	U3104416	4	302.6	300.3
U3103451	7	307.5	300.2	U3103908	6	307.5	300.1	U3104416	5	307.5	300.3
U3103451	8	312.4	300.2	U3103908	7	312.5	300.1	U3104416	6	312.5	300.3
U3103451	9	314.8	300.2	U3103908	8	314.9	300.1	U3104416	7	314.9	300.3
U3103451	10	311.9	300.2	U3103908	9	312.0	300.1	U3104416	8	312.1	300.3
U3103451	11	307.0	300.2	U3103908	10	307.1	300.1	U3104416	9	307.1	300.3
U3103451	12	302.1	300.2	U3103908	11	302.2	300.1	U3104416	10	302.2	300.3
U3103451	13	297.2	300.2	U3103908	12	297.3	300.1	U3104416	11	297.4	300.3
U3103451	14	292.4	300.2	U3103908	13	292.5	300.1				
U3103451	15	282.6	300.2								

Table 8: Specifications addressed in this work [2]

SRV0053	The VIIRS sensor emissive bands shall meet the sensitivity requirments of TABLE 15. (TABLE 15 is listed as Table 9 in this text.)
SRV0545	For the bands specified as moderate resolution and emissive, the absolute radiometric calibration uncertainty of spectral radiance shall be equal to or less than the percentage specified in TABLE 17. (TABLE 17 is listed as Table 10 in this text.)
SRV0546	For the bands specified as imaging and emissive (TABLE 1), given a uniform scene of brightness temperature of 267 K, the calibration uncertainty of spectral radiance shall be as specified in TABLE 18. (TABLE 18 is listed as Table 10 in this text.)
SRV0613	The calibrated output of all channels within a band shall be matched to the band mean output within the NEdL / NEdT (1 sigma) when viewing a uniform scene. The matching condition shall be met between radiance levels from L_{MIN} to 0.9 L_{MAX}.
SRV0654	The sensor shall be capable of maintianing the temperature of the on-board blackbody to within ±0.2 K of the programmed setpoint temperature.
SRV0095	The emitting surface of the VIIRS sensor on-board blackbody source shall have a temperature uniformity of 0.03 K when operated under temperature controlled or unpowered conditions. Temperature uniformity is defined as the standard deviation of the temperatures measured by the sensors embbedded in the OBC BB.

Table 9: Sensitivity requirements for the emissive bands [2]

			Single Gain		Dual Gain			
					High Gain		Low Gain	
Band	Center Wavelength (nm)	Gain Type	T_{TYP}	NEdT	T_{TYP}	NEdT	T_{TYP}	NEdT
M12	3700	Single	270	0.396	~	~	~	~
M13	4050	Dual	~	~	300	0.107	380	0.423
M14	8550	Single	270	0.091	~	~	~	~
M15	10783	Single	300	0.07	~	~	~	~
M16	12013	Single	300	0.072	~	~	~	~
I4	3740	Single	270	2.5	~	~	~	~
I5	11450	Single	210	1.5	~	~	~	~

Table 10: Absolute radiometric calibration uncertainty of the spectral radiance for the emissive bands [2]

Band	Scene Temperature (K)					
	190	230	267	270	310	340
I4	~	~	5.00%	~	~	~
I5	~	~	2.50%	~	~	~
M12	N/A	7.00%	~	0.70%	0.70%	0.70%
M13	N/A	5.70%	~	0.70%	0.70%	0.70%
M14	12.30%	2.40%	~	0.60%	0.40%	0.50%
M15	2.10%	0.60%	~	0.40%	0.40%	0.40%
M16	1.60%	0.60%	~	0.40%	0.40%	0.40%

Figure 1: a_0 coefficient versus detector

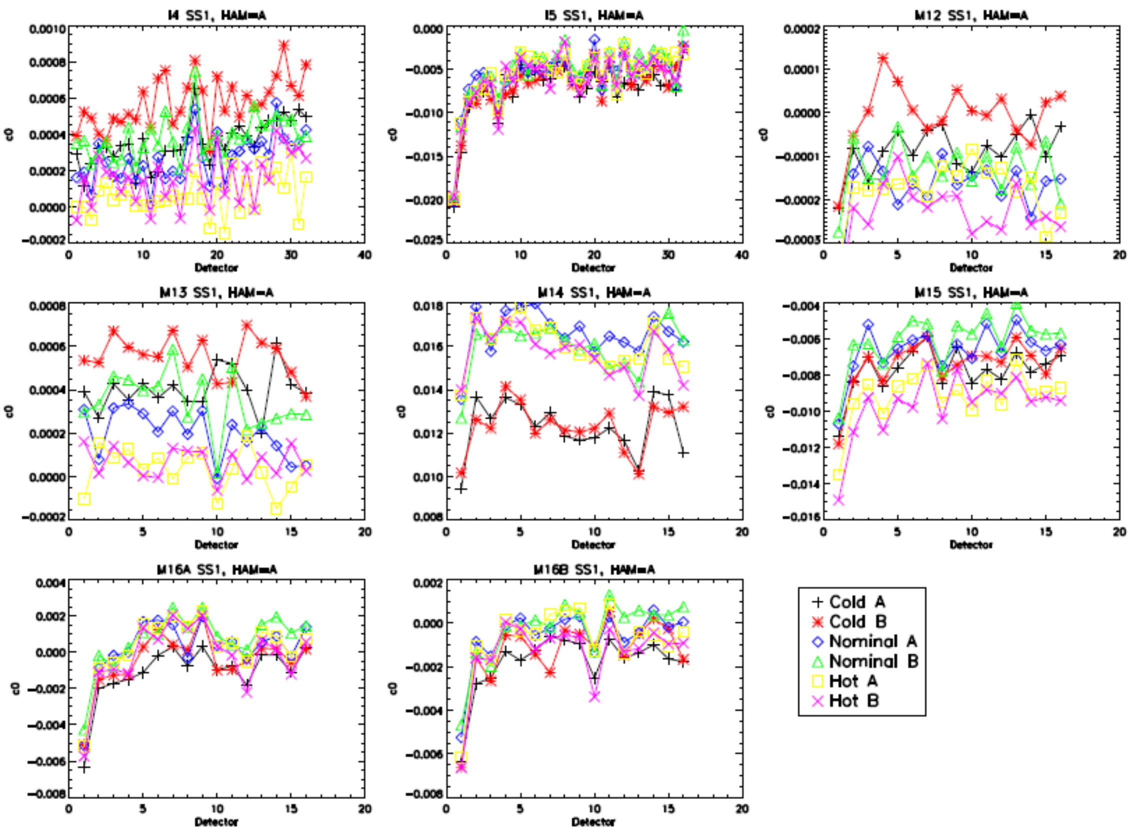

Figure 2: a_0 coefficient versus T_{OMM} (all detectors)

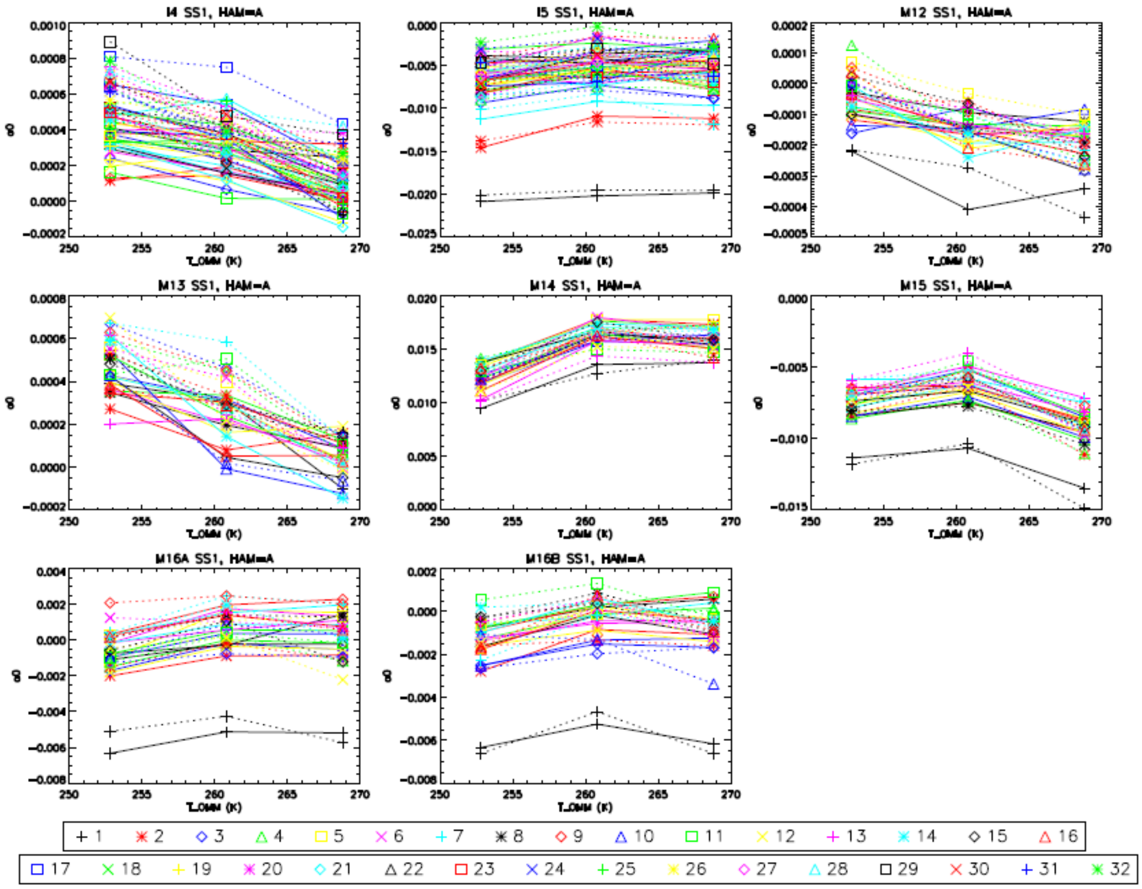

Figure 3: a_0 versus T_{OMM} (middle detector with 2 sigma error bars)

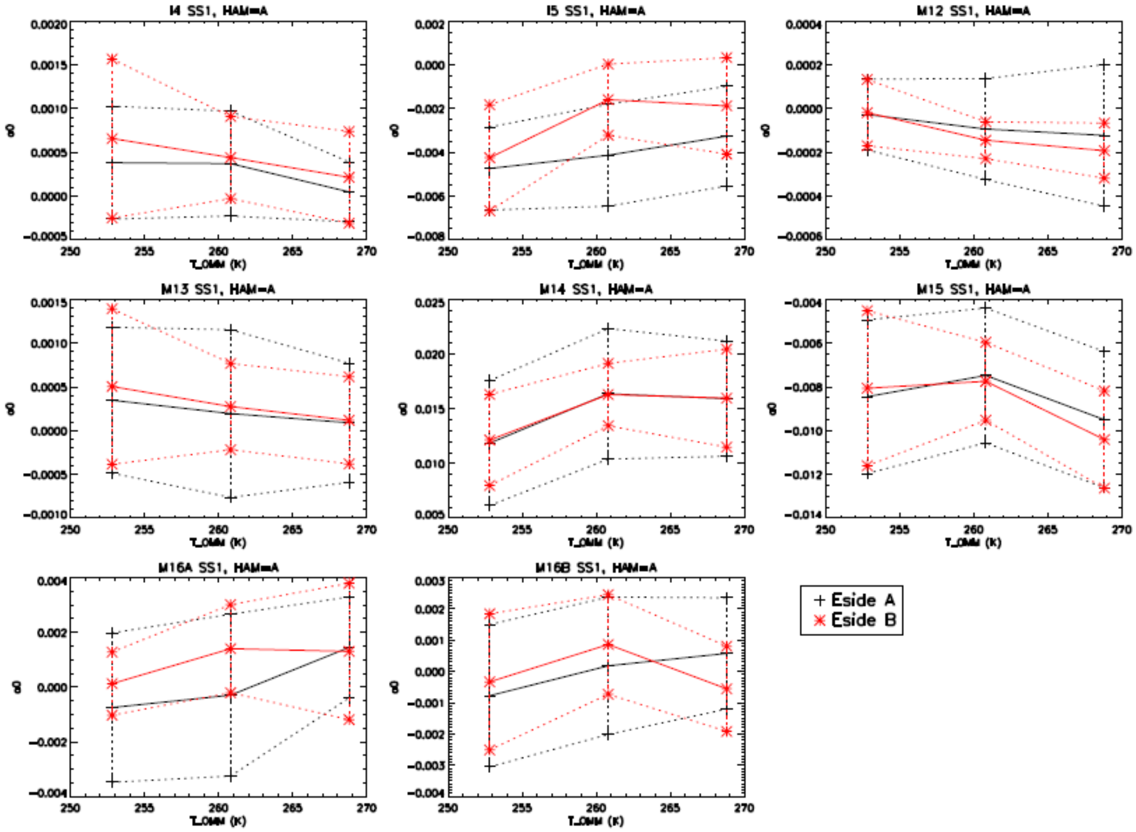

Figure 4: $1/a_1$ coefficient versus detector

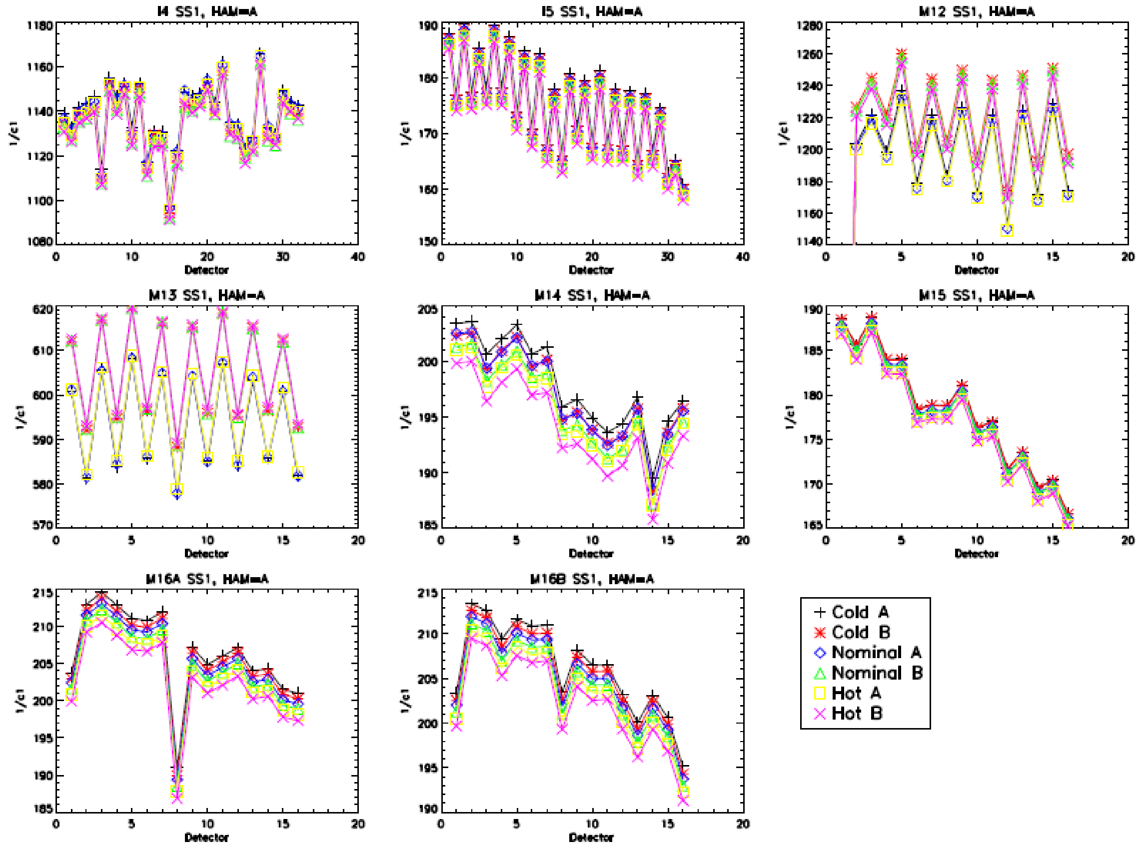

Figure 5: $1/a_1$ coefficient versus T_{OMM} (all detectors)

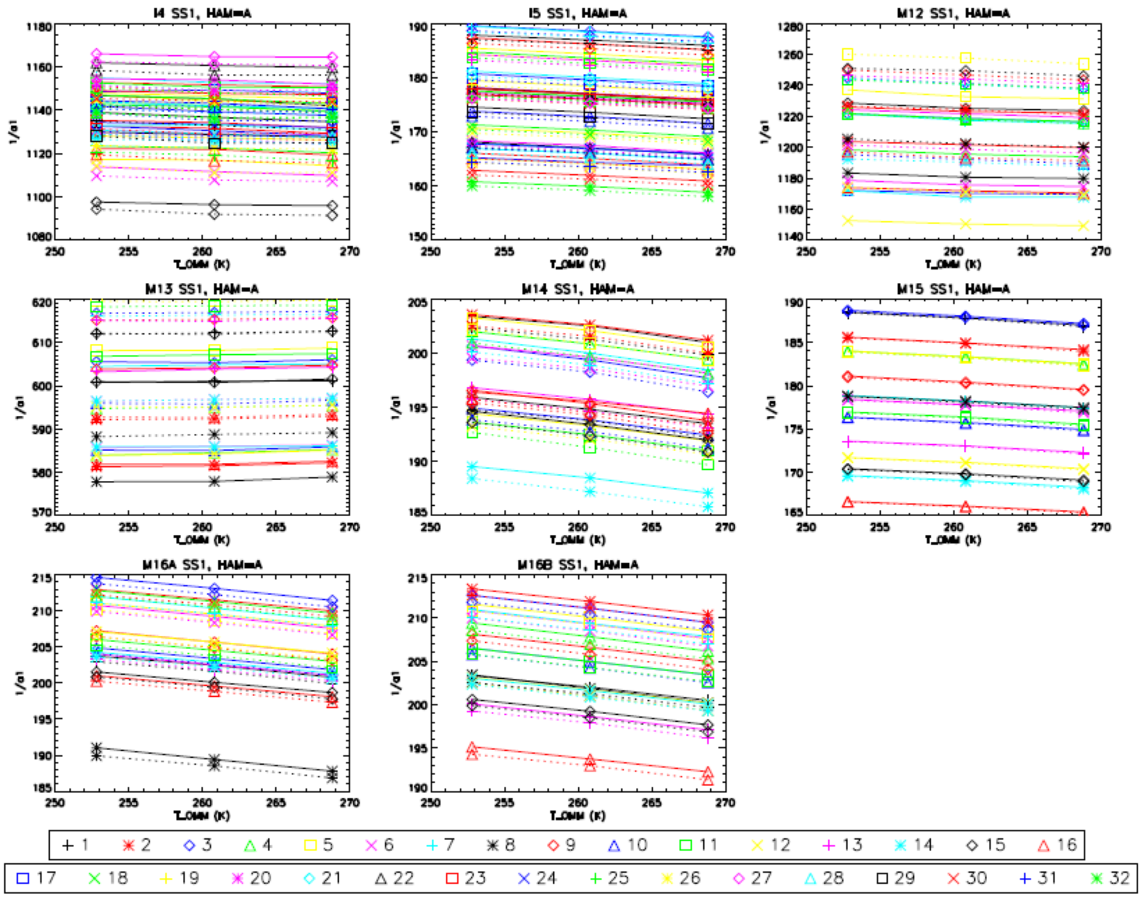

Figure 6: $1/a_1$ versus T_{OMM} (middle detector with 2 sigma error bars)

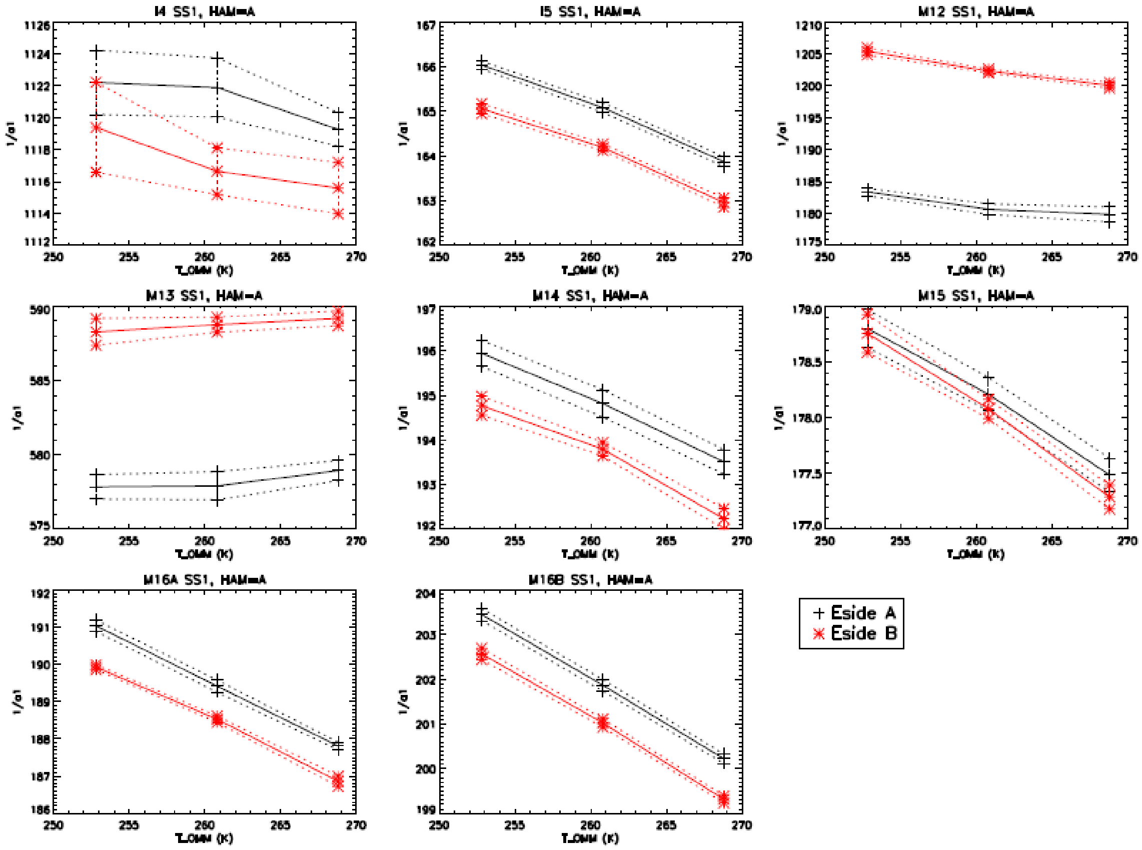

Figure 7: a_2 coefficient versus detector

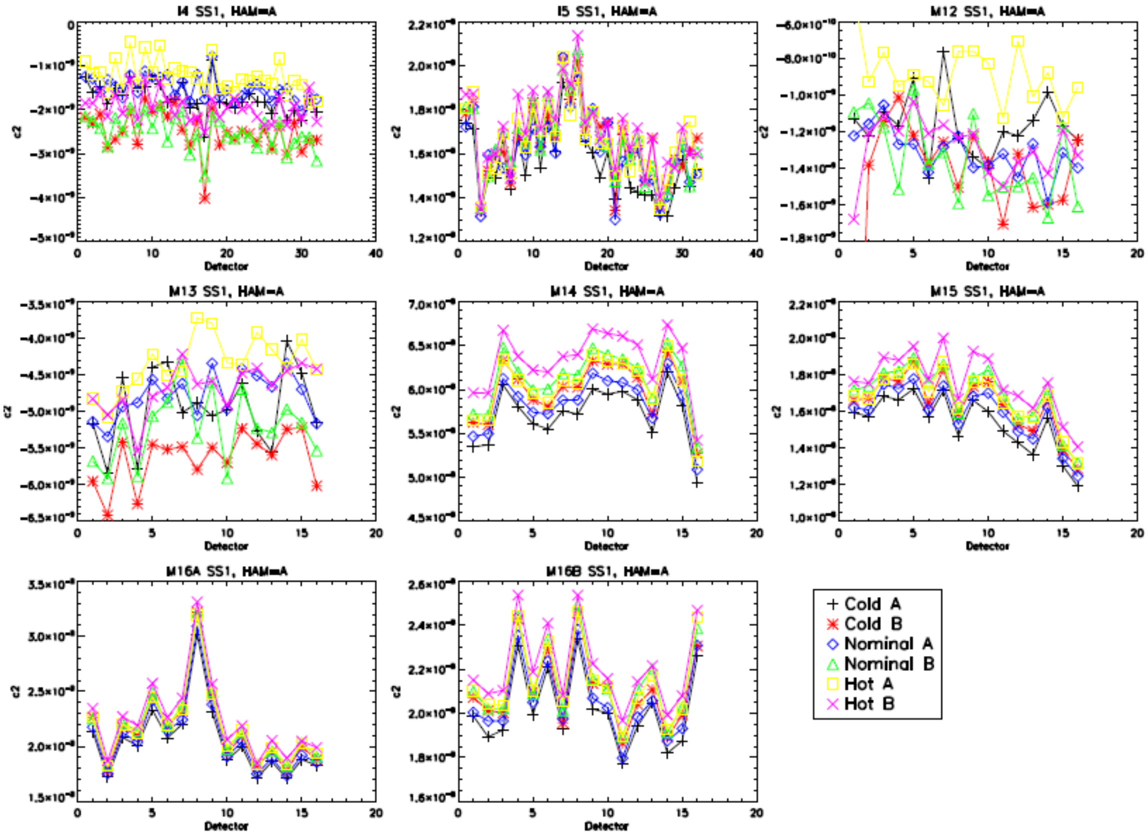

Figure 8: a_2 coefficient versus T_{OMM} (all detectors)

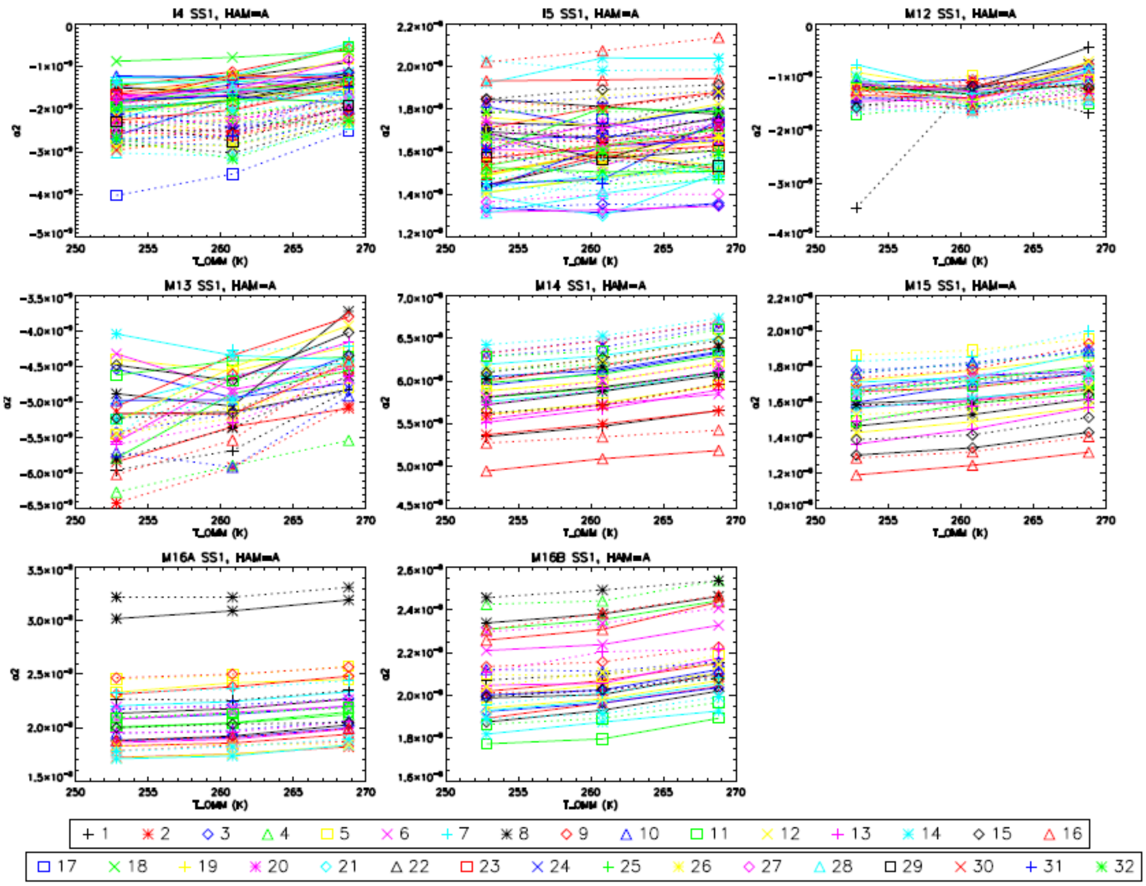

Figure 9: a_2 versus T_{OMM} (middle detector with 2 sigma error bars)

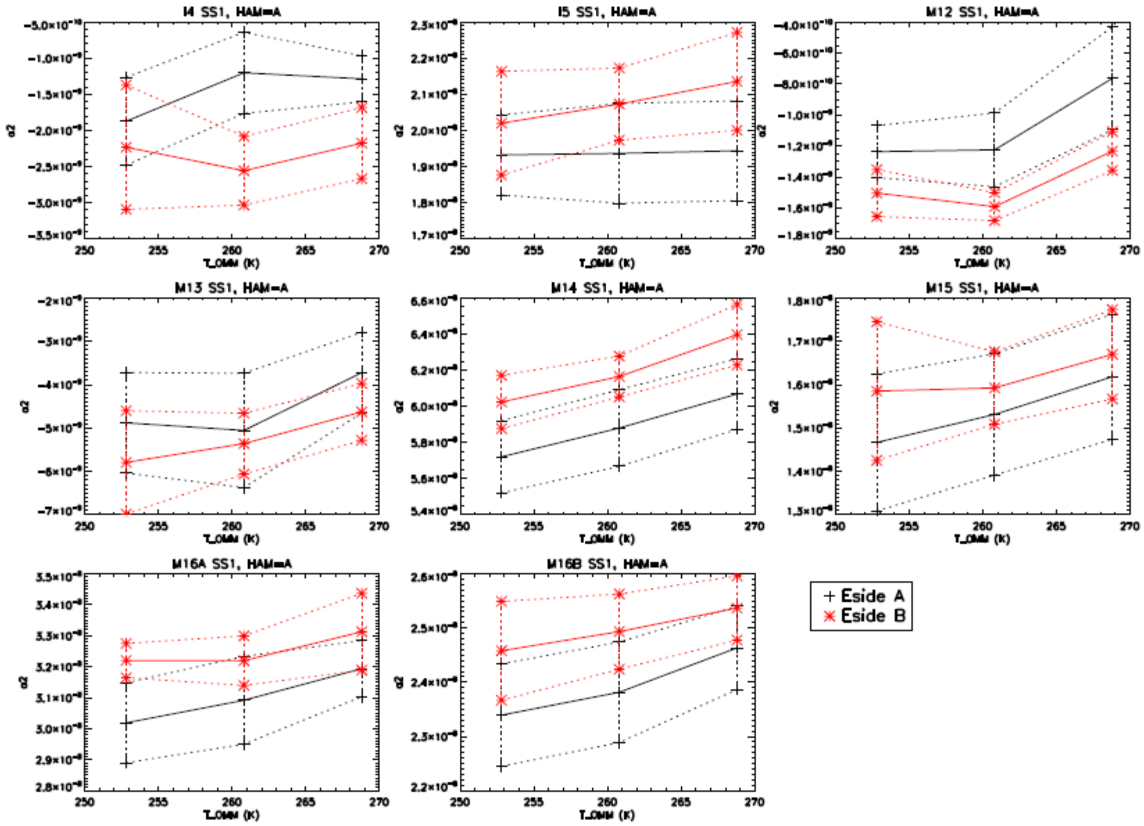

Figure 10: NEdT at T_{TYP} versus detector

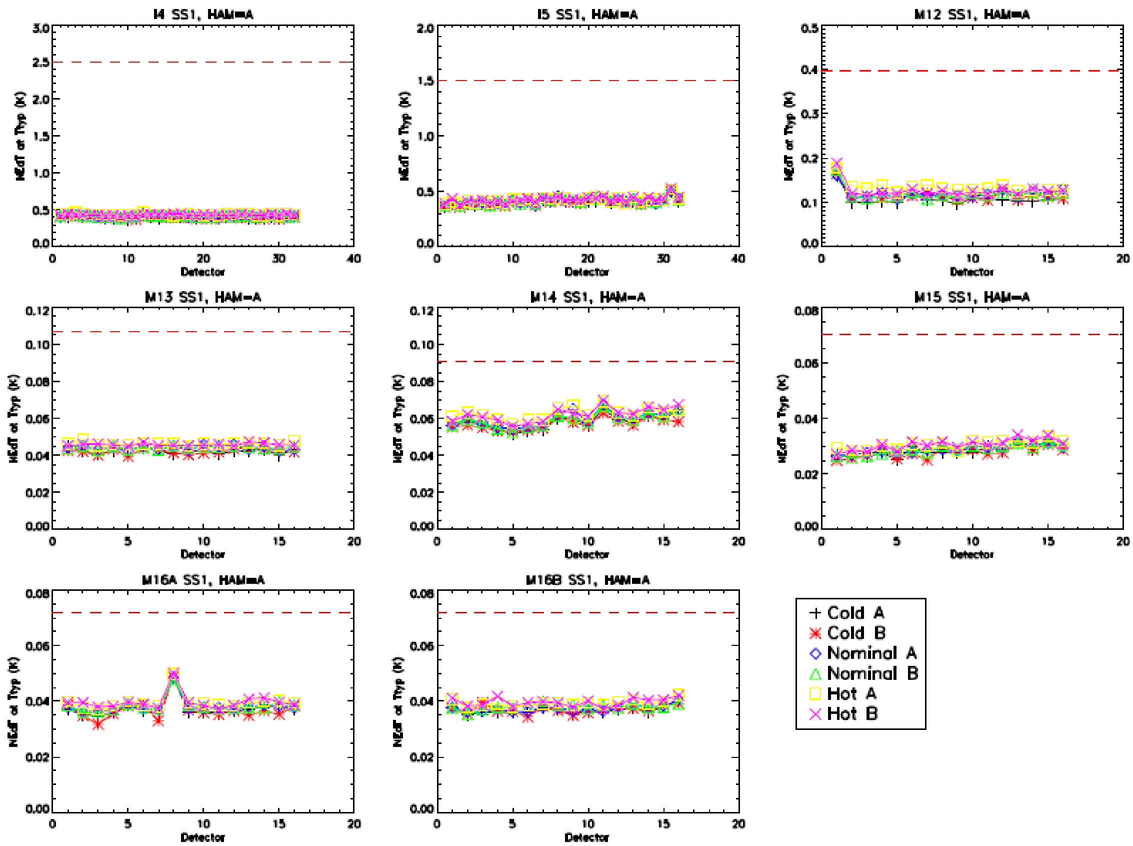

Figure 11: NEdT at T_{TYP} versus T_{OMM} (all detectors)

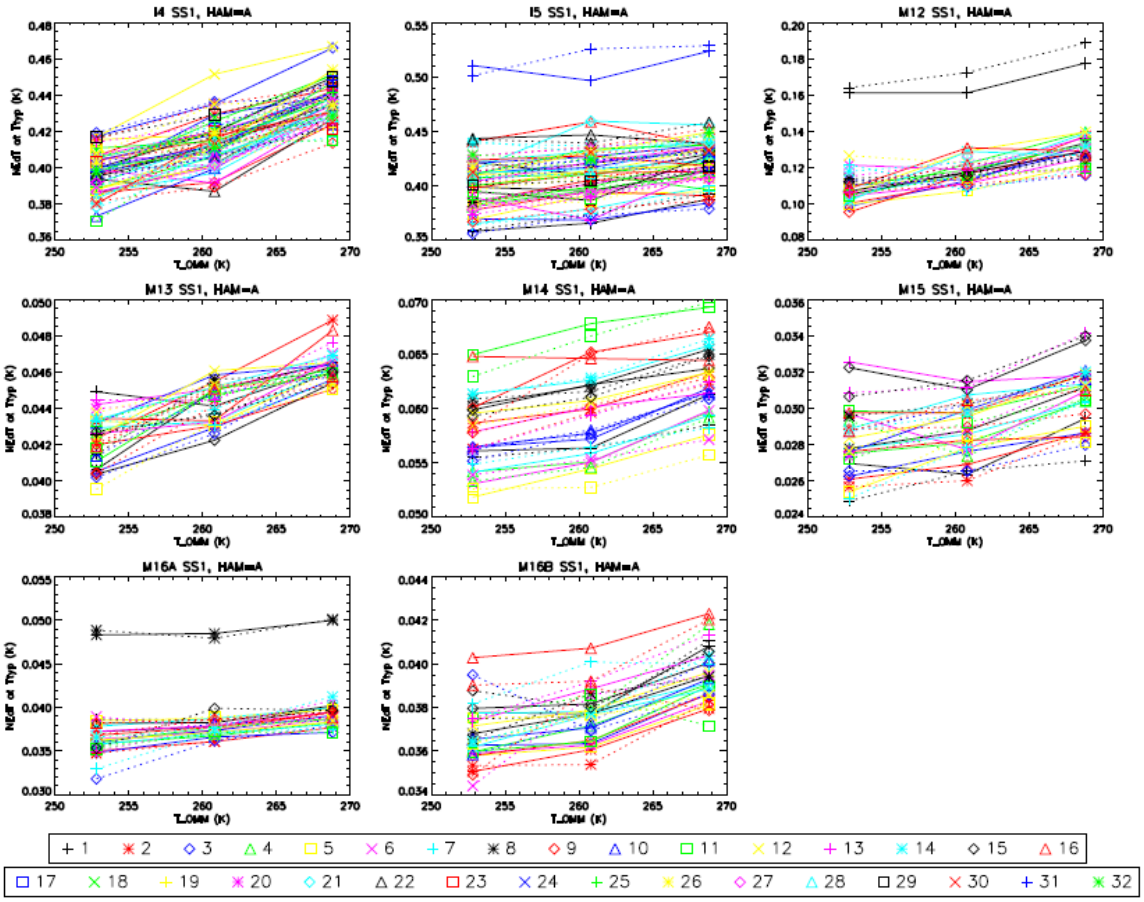

Figure 12: NEdT versus T_{BCS} (median detector)

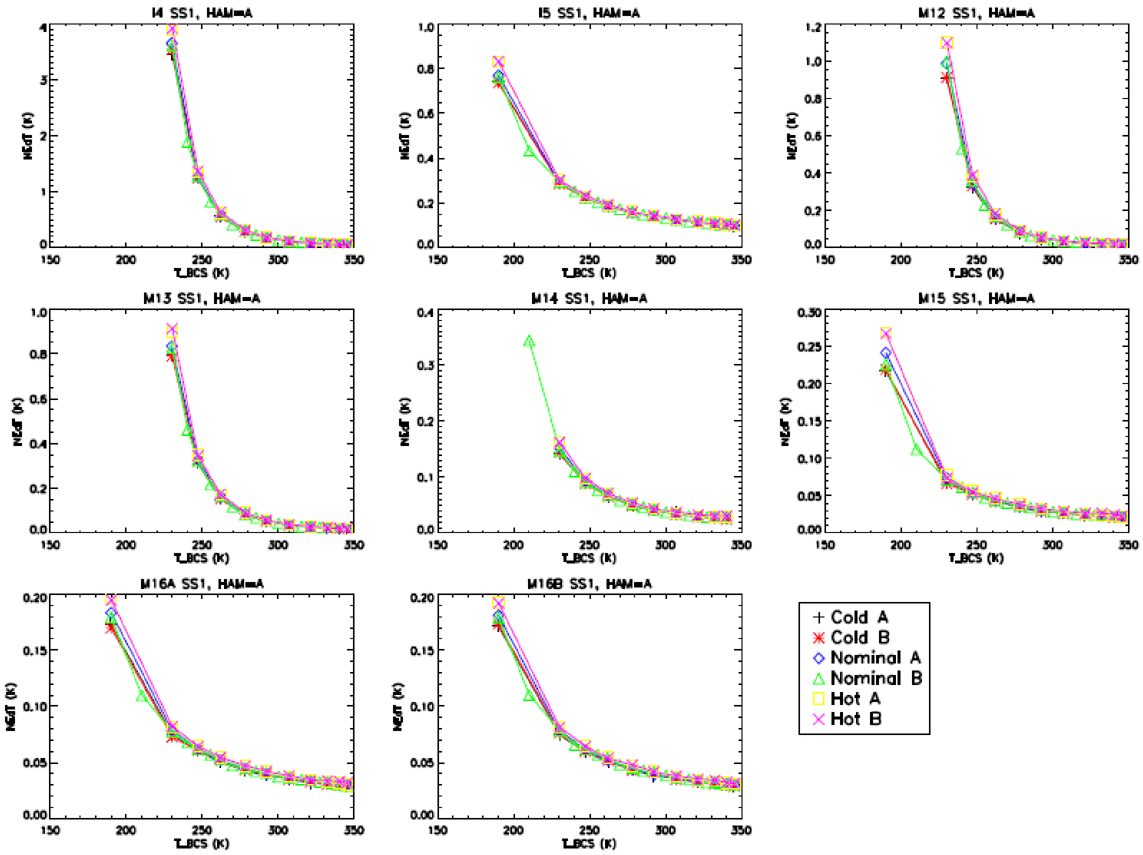

Figure 13: RRNL versus detector

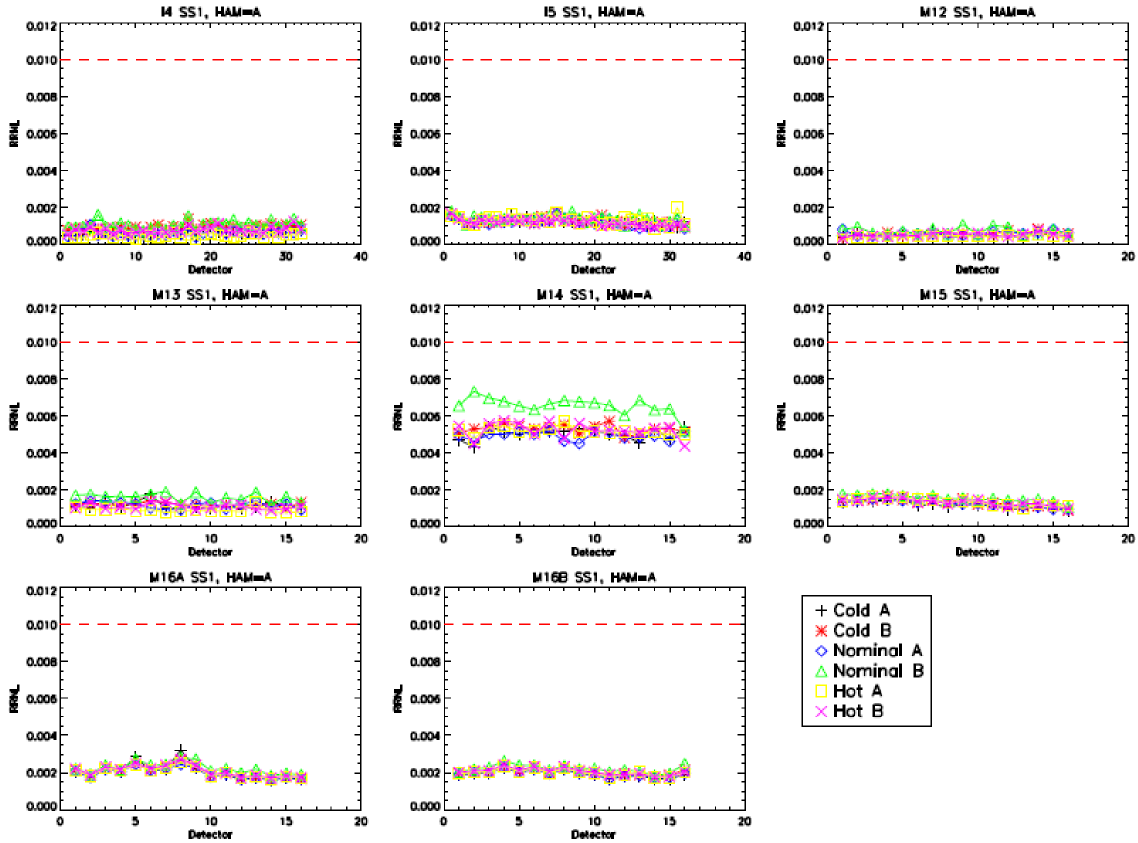

Figure 14: ARD versus T_{BCS} (median detector)

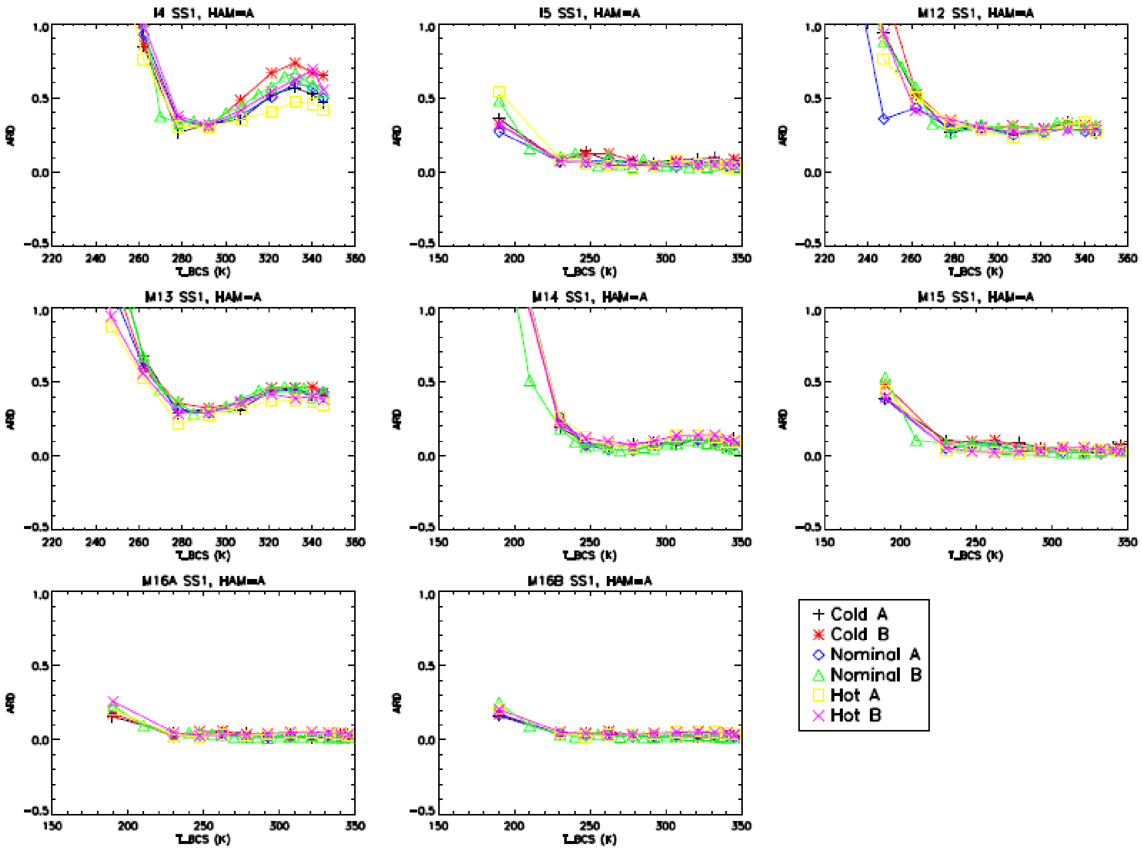

Figure 15: RRU versus T_{BCS} (median detector)

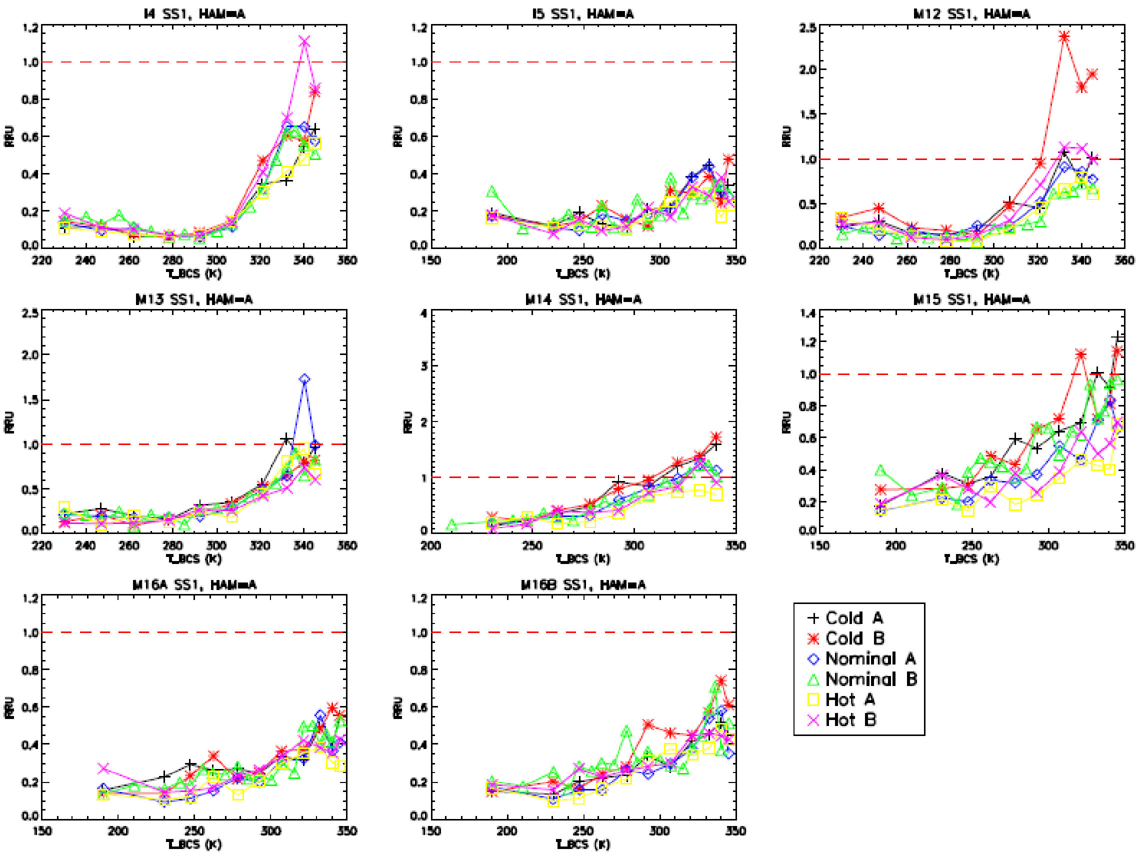

Figure 16: M13 low gain coefficients versus detector

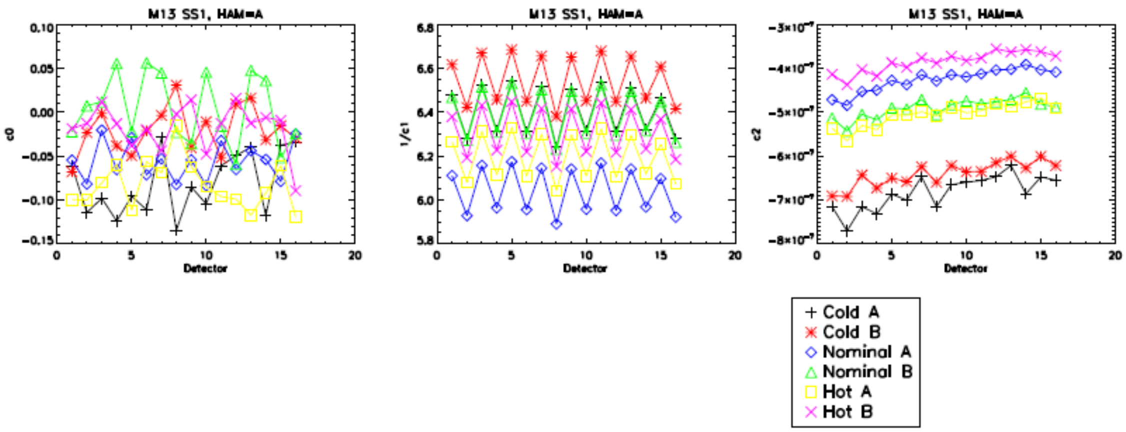

Figure 17: M13 low gain coefficients versus T_{OMM} (all detectors)

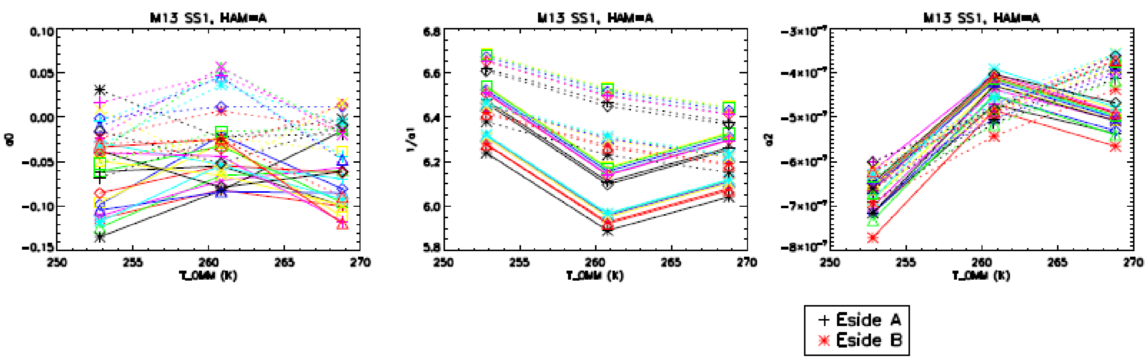

Figure 18: M13 low gain coefficients versus T_{OMM} (middle detector with 2 sigma error bars)

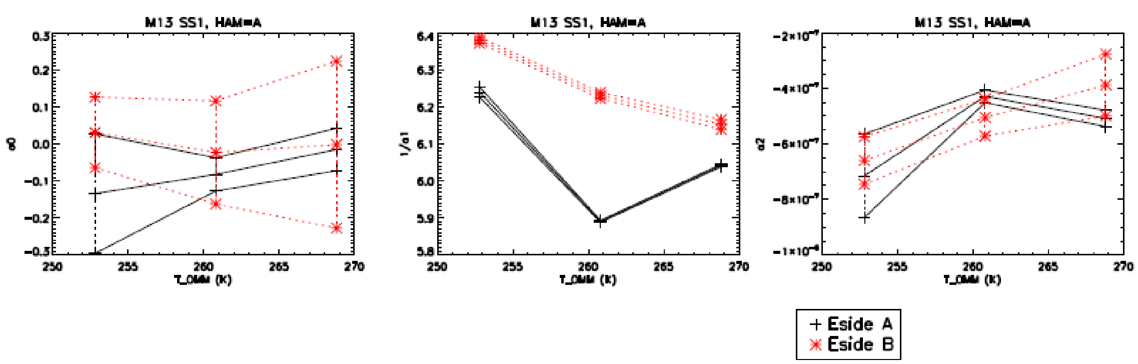

Figure 19: NEdT at T_{TYP} versus detector as well as NEdT versus T_{TMC} (median detector)

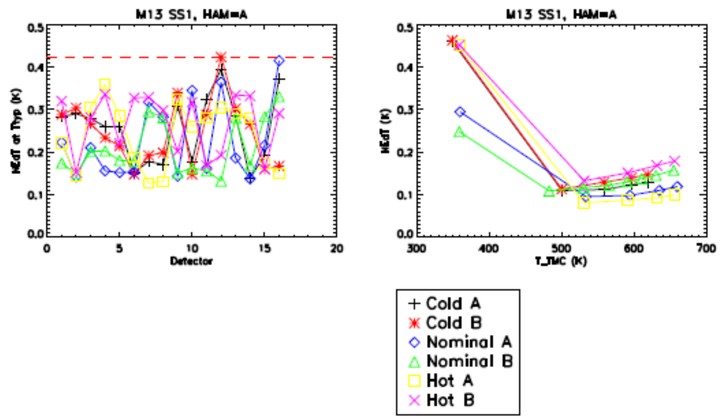

Figure 20: RRNL versus detector as well as ARD and RRU versus T_{TMC} (median detector)

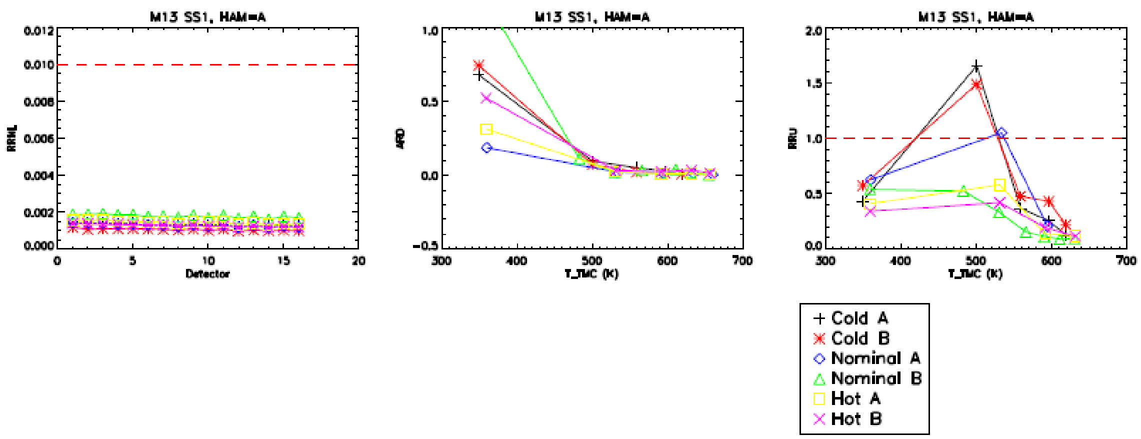

Figure 21: a_0 coefficient versus detector from warm up

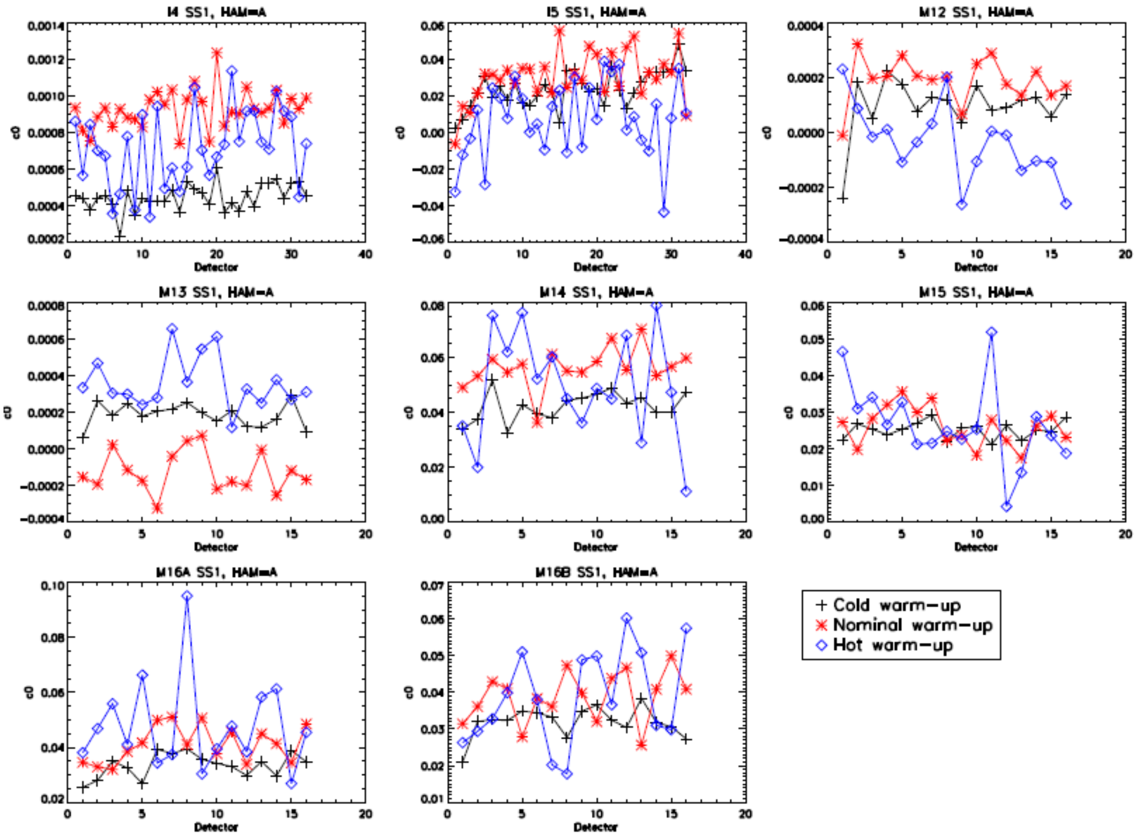

Figure 22: a_0 coefficient versus T_{OMM} from warm up (median detector)

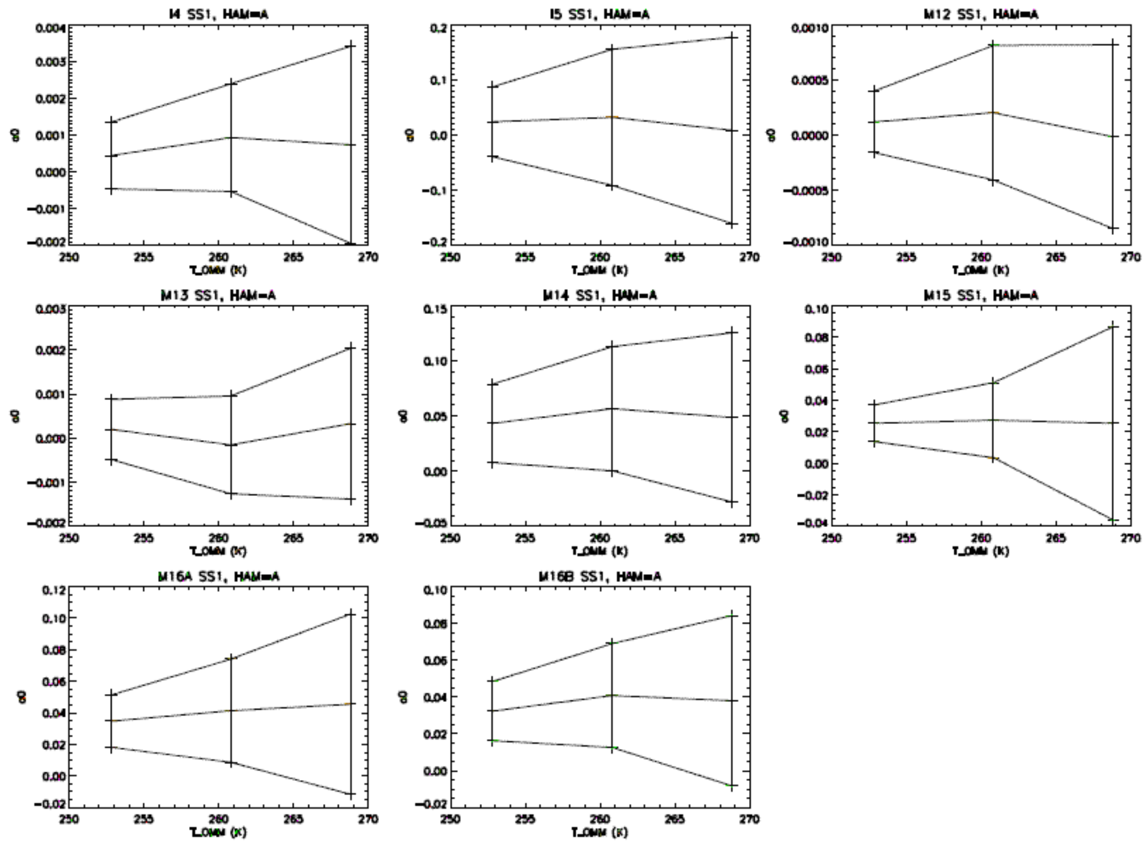

Figure 23: $1/a_1$ coefficient versus detector from warm up

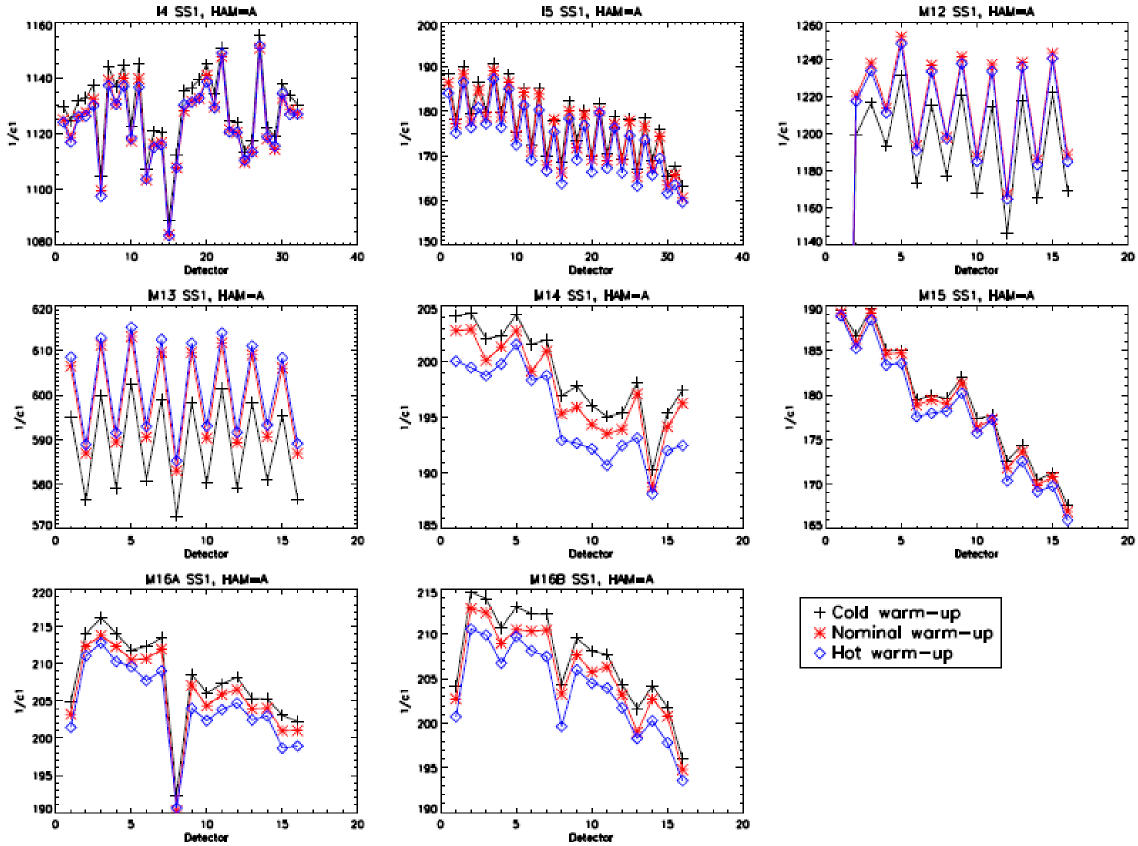

Figure 24: $1/a_1$ coefficient versus T_{OMM} from warm up (median detector)

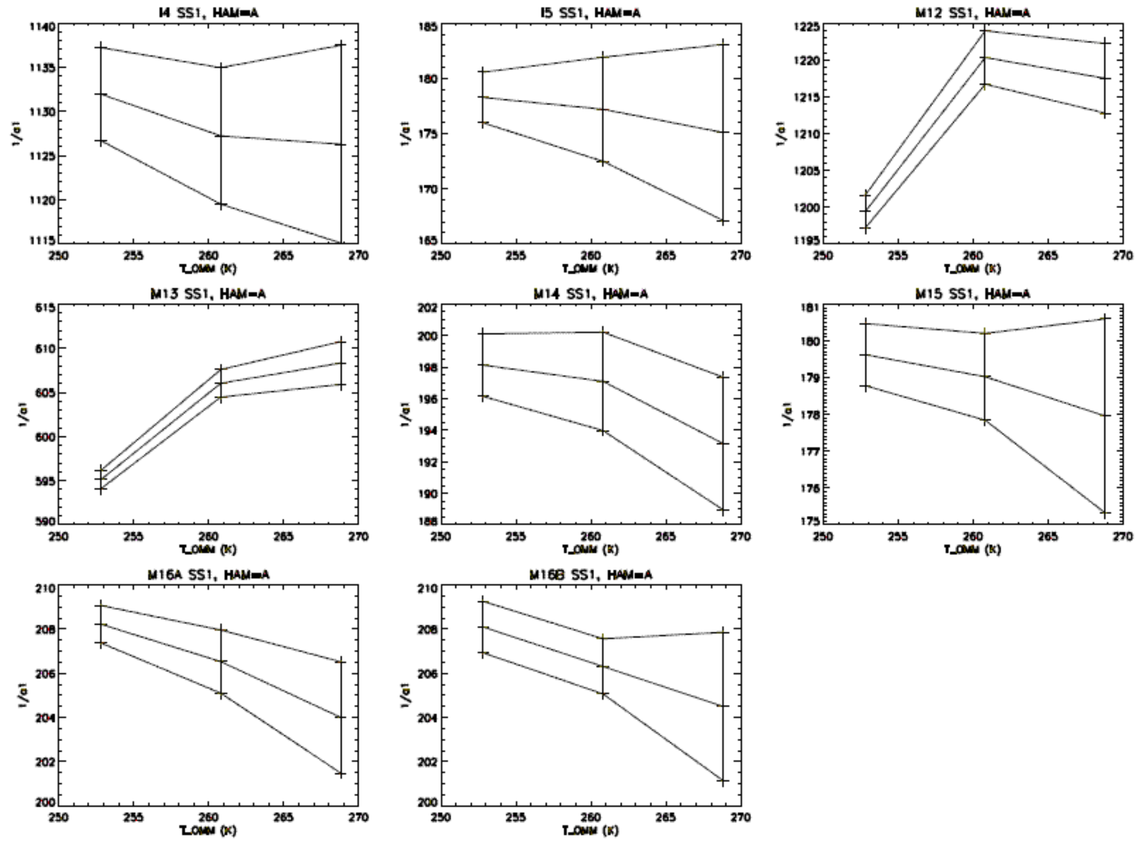

Figure 25: a_2 coefficient versus detector from warm up

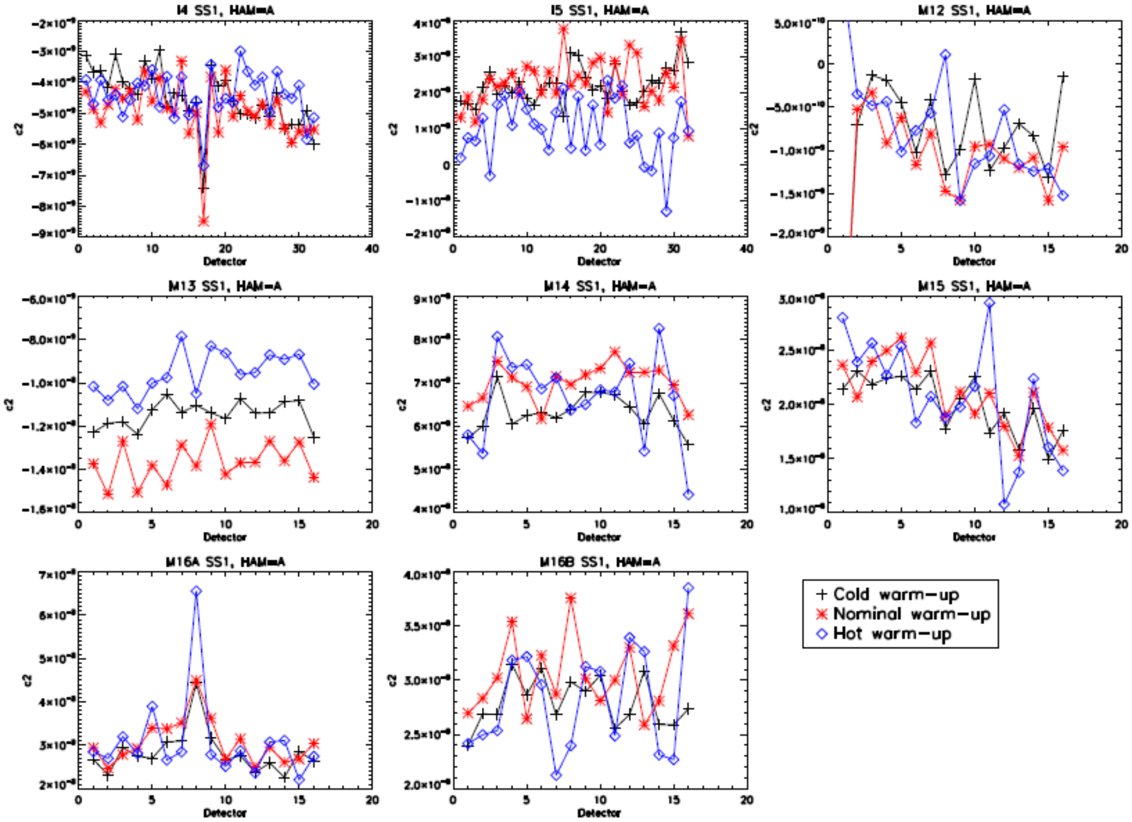

Figure 26: a_2 coefficient versus T_{OMM} from warm up (median detector)

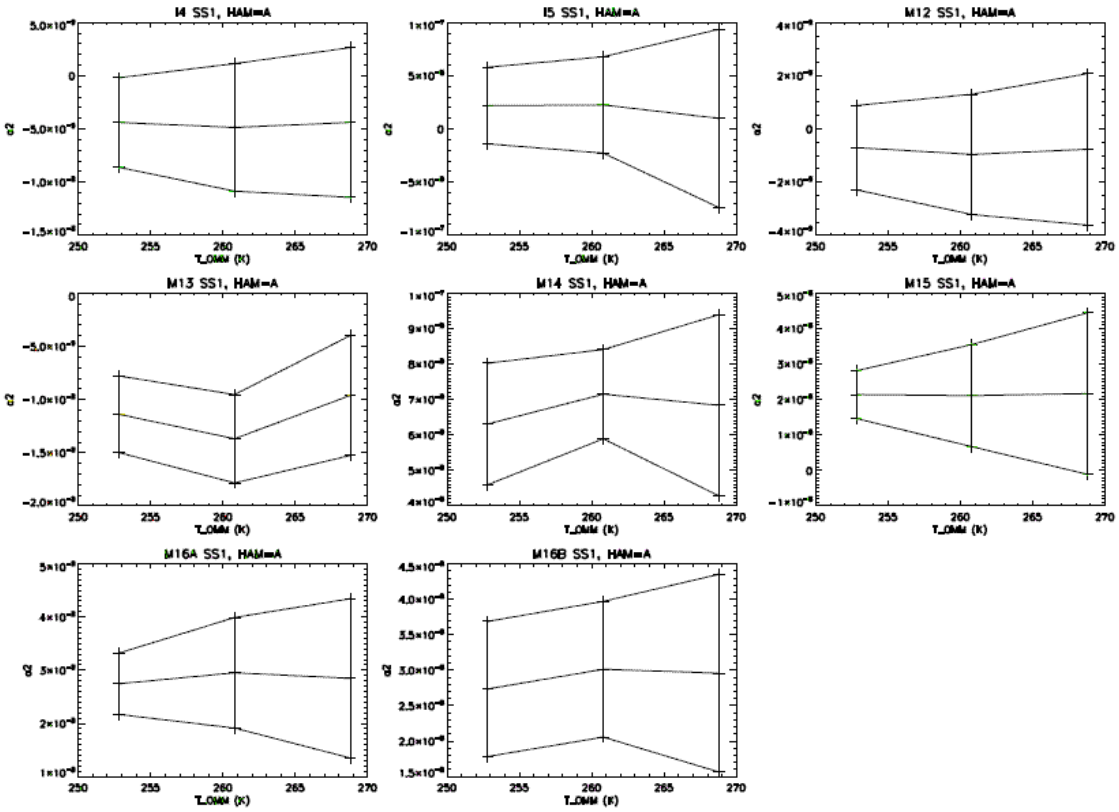

Figure 27: $1/a_1$ coefficient versus detector from cool down

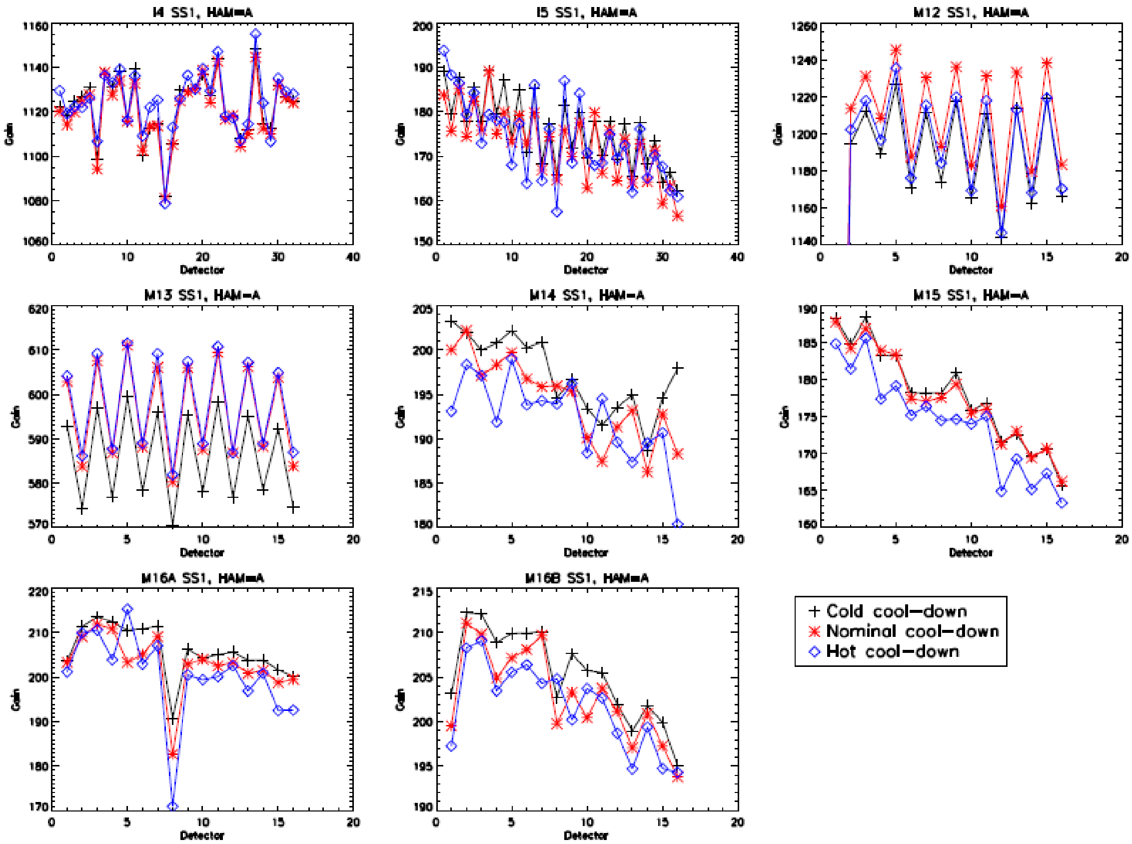

Figure 28: NEdT at T_{TYP} versus detector

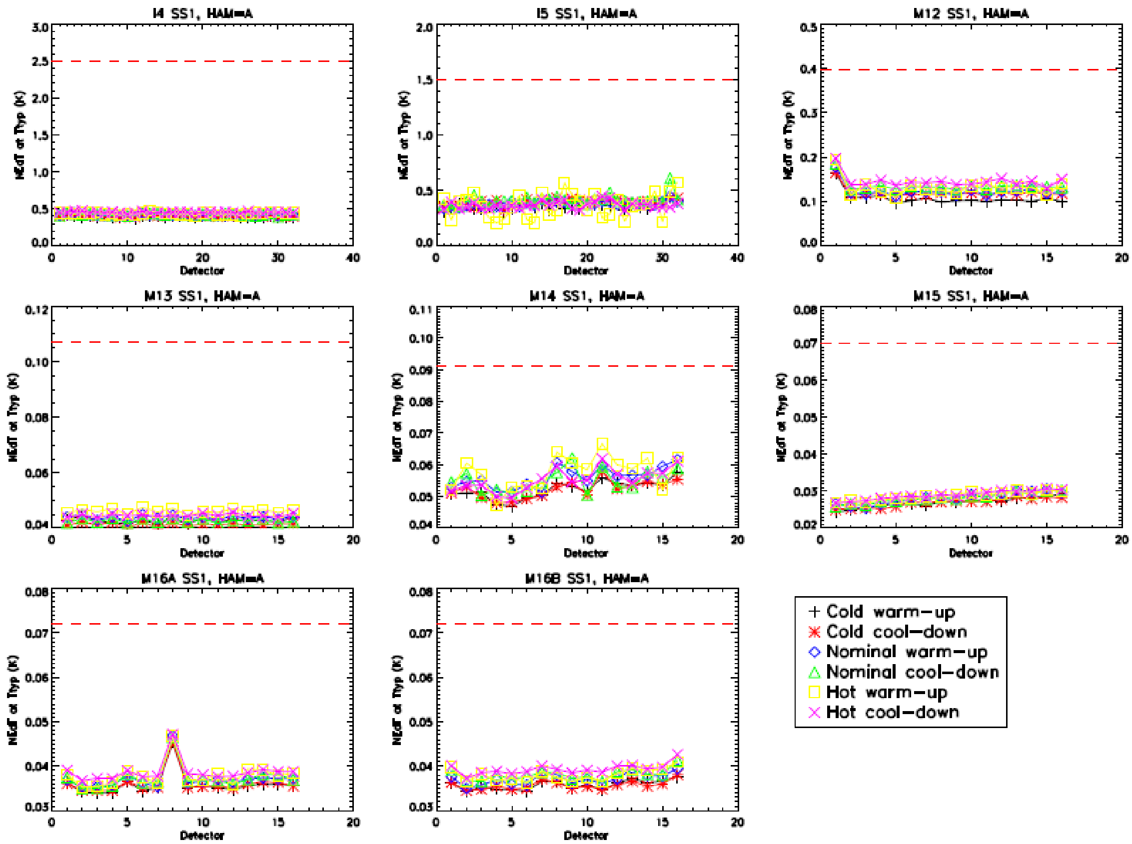

Figure 29: BCS ARD versus T_{OBC} (median detector)

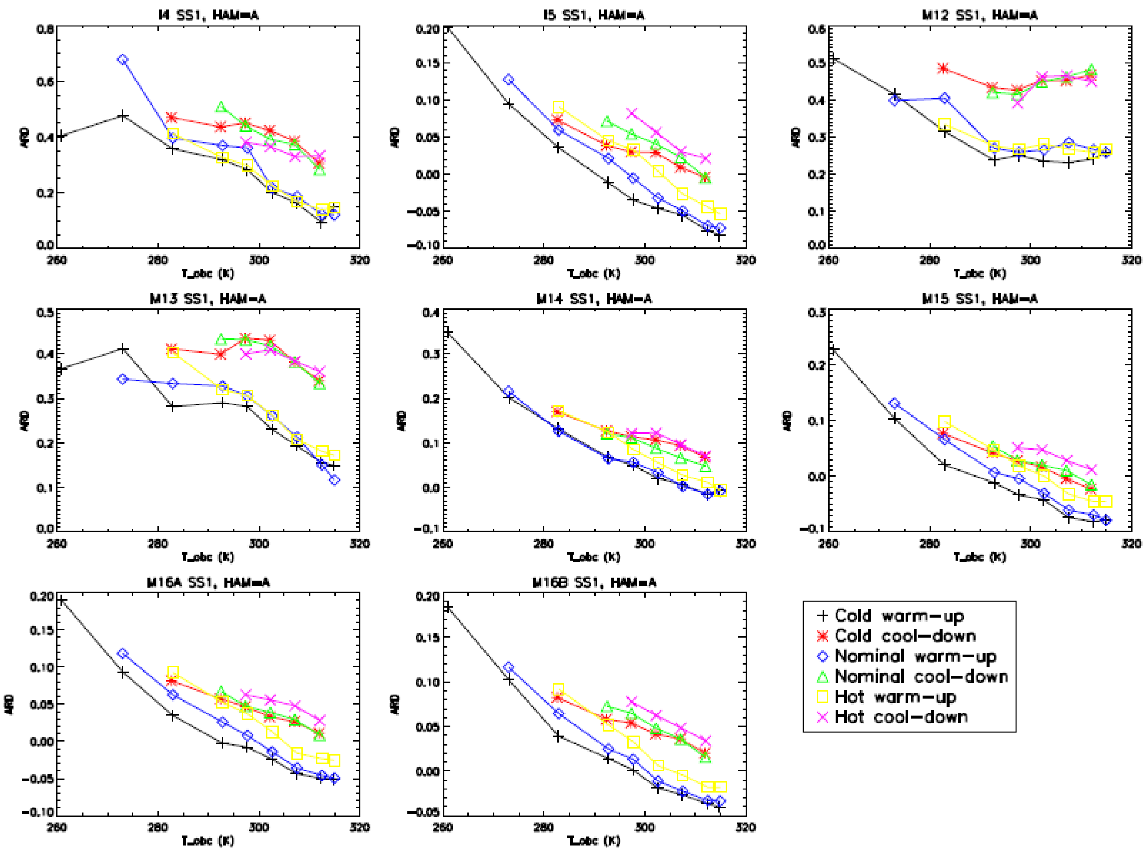

Figure 30: Deviation of T_{OBC} from OBC setpoint

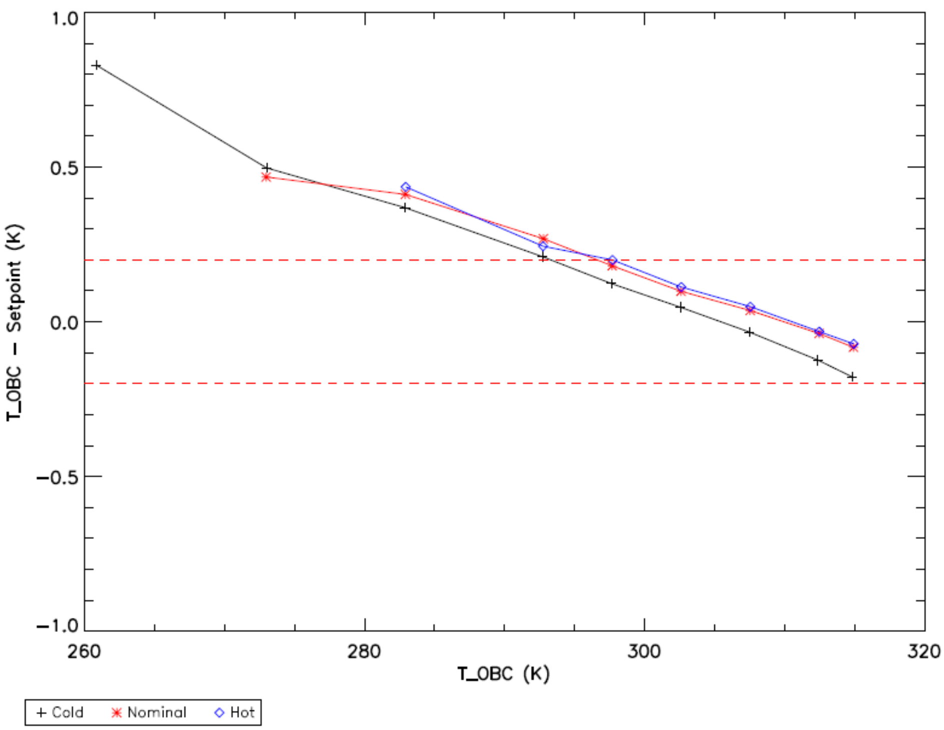

Figure 31: Standard Deviation of the six OBC thermistors versus T_{OBC}